The cellular diversity of human cerebrospinal fluid following intraventricular hemorrhage revealed by single-nucleus RNA sequencing

Sonia Malaiya[1,2]*, Riccardo Serra[3]*, Marcia Cortes-Gutierrez[1]*, Bradley E. Wilhelmy[4], Emily Jusuf[5,6], Mayur Somalinga[5], Dave Peprah[5], Hirschel Nambiar[5], Kevin T. Kim[3], Jordan R. Saadon[3], Parantap D. Patel[3], Steven K. Yarmoska[3], Maureen Rakovec[3], John Kim[3], Catherine Lei[3], Shreyas Panchagnula[3], Reina Ambrocio[7], Meagan Cherney[8], Nicholas A. Morris [5,7], Natarajan Ayithan[9], Xiaoxuan Fan[9], Volodymyr Gerzanich[3], J. Marc Simard[3], Neeraj Badjatia[5,7], Gary Schwartzbauer[3,5], Gunjan Y. Parikh[5,7], Seth Ament[1,10,11‡], Prajwal Ciryam[5,7,11‡]

*These authors contributed equally.

‡To whom correspondence should be addressed: sament@som.umaryland.edu, pciryam@som.umaryland.edu

1. Institute for Genome Sciences, University of Maryland School of Medicine, Baltimore, USA.
2. Program in Neuroscience, University of Maryland School of Medicine, Baltimore, USA.
3. Department of Neurosurgery, University of Maryland School of Medicine, Baltimore, USA.
4. Department of Neurosurgery, The Ohio State University, Columbus, USA.
5. Program in Trauma, University of Maryland Shock Trauma Center, Baltimore, USA.
6. Renaissance School of Medicine, Stony Brook University, Stony Brook, USA.
7. Department of Neurology, University of Maryland School of Medicine, Baltimore, USA.
8. University of Maryland Medical Center, Baltimore, USA.
9. Department of Microbiology and Immunology, University of Maryland School of Medicine, Baltimore, USA.
10. Maryland Psychiatric Research Center, Department of Psychiatry, University of Maryland School of Medicine, Baltimore, USA.
11. UM-MIND Institute for Neuroscience Discovery, University of Maryland School of Medicine, Baltimore, USA.

Abstract

Background. Intraventricular hemorrhage (IVH) is a common and severe complication of hemorrhagic brain injury. Current treatments offer limited improvement in long-term neurological outcomes. Inflammatory responses in the cerebrospinal fluid (CSF) after IVH are thought to drive secondary injury, but the cellular mechanisms underlying this inflammation remain poorly defined.

Methods. We performed single-nucleus RNA sequencing of leukocytes isolated from CSF collected through external ventricular drains in subjects with intracerebral (n = 6) or subarachnoid (n = 1) hemorrhage. We characterized transcriptionally distinct subpopulations of neutrophils, monocytes, and lymphocytes by comparison to reference datasets. Cell–cell signaling networks were analyzed to infer cytokine-mediated communication, and a flow cytometry panel was developed to validate transcriptomic findings in independent CSF samples.

Results. We obtained 11,191 high-quality nuclei comprising neutrophils (53.8%), monocytes (26.1%), lymphocytes (17.8%), and non-immune cells (2.4%). Neutrophils segregated into Nascent, Quiescent, and Interferon-Activated states. Monocytes exhibited classical phenotypes that include interferon-activated states (characterized by expression of *VCAN* or *PROK2*) and CXC-chemokine expressing states (characterized by expression of *CXCL5* or *CXCL8*). Lymphocytes were mainly naïve and central memory $CD4^+$ T cells. Cell–cell signaling analysis predicted strong CXC chemokine signaling from monocytes to neutrophil subsets and IL-1 family–driven inflammatory responses across multiple populations. Type I and III interferon signaling defined a neutrophil population not previously described in the central nervous system.

Conclusion. This study delineates the diverse cellular immune landscape of CSF after IVH. Transcriptomic profiles reveal interferon, IL-1, and CXC chemokine signaling networks as potential therapeutic targets to mitigate secondary injury.

Introduction

53 Bleeding into the cerebral ventricles, known as intraventricular hemorrhage (IVH), is an ominous complication of
54 hemorrhagic brain diseases, including intracerebral hemorrhage (ICH), subarachnoid hemorrhage (SAH), and
55 traumatic brain injury (TBI). In adults, it results in death or severe disability in over 50% of cases[1]. The
56 development of elevated intracranial pressure and hydrocephalus contribute to morbidity and mortality[2–4].
57 Treatment options are limited, and while around 50% of patients require temporary drainage of cerebrospinal
58 fluid (CSF) with an external ventricular drain (EVD)[5,6], lifelong CSF shunting via ventriculoperitoneal shunting is
59 needed in up to 40% of subjects[7,8]. Intraventricular injection of tissue plasminogen activator does not improve
60 functional outcomes or reduce the rate of shunting[7].

61

62 As new prognostic and treatment approaches are sought for this morbid disease, promising strategies may arise
63 from the critical role of inflammation in IVH. The deposition of blood into the cerebral ventricles stimulates a
64 profound inflammatory response that recruits leukocytes into the central nervous system[9,10]. In the first several
65 days after injury, this response is dominated by myeloid cells: first neutrophils, then monocytes and macrophages.
66 These cells interact with CNS resident cells, with both pathological and reparative consequences. On one hand,
67 inflammation after IVH can cause neuronal injury, cerebral edema, and hydrocephalus; on the other, it may
68 stimulate neurogenesis and clearance of hemorrhagic debris[11–14]. Because of the numerous and pleiotropic
69 contributors to inflammation in IVH, comprehensive approaches are needed to characterize this process.

70

71 Here, we sought to characterize the CSF inflammatory response in patients after IVH, using single-nucleus RNA
72 sequencing. Our approach identified distinct states of neutrophils and monocytes in the CSF, including a
73 population of interferon-induced neutrophils not previously described in the central nervous system. These
74 findings illustrate the complex cellular inflammatory response to IVH and point to potential novel therapeutic
75 targets for further investigation.

76

77 **Results**

78 ***A snRNA-seq atlas for cellular diversity of ventricular CSF in the context of intraventricular hemorrhage.***

79 Previous scRNA-seq studies of CSF samples from patients with IVH did not capture its full cellular diversity.
80 Based on prior CSF cell count data in IVH[15], we anticipated that the CSF samples we collected would be highly
81 represented in neutrophils and other fragile populations that could be depleted during sample processing. We
82 reasoned that single-nucleus RNA sequencing (snRNA-seq) could provide a means to limit these processing-
83 induced biases and might yield a more representative cellular atlas of IVH. We obtained ventricular CSF of seven
84 study participants who presented with IVH, either directly to the University of Maryland Medical Center or after
85 emergent transfer from another institution (**Fig. 1A**; **Table 1**). Six subjects presented after ICH, with etiologies
86 including hypertension and coagulopathy/anticoagulation-related hemorrhage, with one subject whose etiology
87 was unknown. One subject presented with aneurysmal SAH. Of the seven subjects, five presented with severe
88 deficits in level of consciousness as quantified by Glasgow Coma Scale (GCS) between 3-8 and two presented
89 with a mild deficit (GCS 13-15). Standardized scales of disease severity were consistent with moderate to severe
90 disease. For subjects with ICH, hemorrhages originated in deep structures of the brain in a majority of cases. All
91 subjects had IVH, either at presentation or subsequently in their hospital course. When CSF is obtained for
92 clinical purposes, excess fluid that would otherwise be discarded is sometimes available. We collected this CSF
93 immediately after it was aspirated. As these are convenience samples, they were obtained at a range of time
94 points after disease onset. Non-contrast CT scans of the head from these subjects demonstrate the presence
95 of IVH and show the EVD tip in the lateral ventricles near the foramen of Monro (**Fig. 1B**). CSF is therefore
96 sampled directly from the ventricles, unlike lumbar puncture, which samples CSF from the lumbar cistern in the
97 lower back. CytoSpin cytology data available from the electronic health record for sample aliquots from five of
98 the seven patients indicated extensive infiltration of leukocytes into the CSF, primarily comprised of neutrophils,
99 monocytes/macrophages, and T cells (**Fig. 1C**).
100
101 snRNA-seq of CSF from these seven study participants yielded 11,191 high-quality nuclear transcriptomes (**Fig.**
102 **2A, B**). Neutrophils (n = 6,017; *S100A8*$^+$, *CXCR1*$^+$, *FCGR3A*$^+$, *FCGR3B*$^+$) were the most abundant cell type,
103 followed by monocytes (n = 2,920; *VCAN*$^+$, *CXCL8*$^+$, *CCL2L1*$^+$), and lymphocytes (n = 1,990; *CD247*$^+$) (**Table**
104 **S1**). We also identified a small number of cells expressing glial or neuronal markers (n = 264; e.g., *PTPRD,*
105 *RSPO3, FLT1, CLDN10, RYR2, RBFOX1, DLG2*) (**Fig 2C**). These cells may derive from damage to the cerebral
106 grey matter during or after the placement of the EVD and were not analyzed further. Cell type proportions

identified by snRNA-seq were in the same range as those obtained using CytoSpin columns (**Fig. 1C**), although our pooling strategy does not allow us to match individual samples across the two technologies. Overall, our data represent a relatively unbiased atlas for the cellular diversity of the CSF in the context of IVH.

Participants' cells were preserved for snRNA-seq processing by two different methods, comparing distinct cell processing protocols in which nuclei were isolated directly from frozen cell pellets vs. cells that had been cryopreserved with DMSO and briefly thawed. snRNA-seq of nuclei derived from pelleted vs. cryopreserved cells yielded a larger number of nuclei from the cryopreservation method, but this method also produced lower RNA counts per nucleus and higher mitochondrial counts per nucleus (**Fig. 2B, Fig. S1 A-C**). The library derived from cryopreserved cells contained a smaller fraction of neutrophils and larger fraction of lymphocytes. It is unclear whether these differences correspond to biological variation among the participants, or whether they reflect a greater vulnerability of neutrophils during cryopreservation and thawing. Nevertheless, these data suggest that all of the cell types in the CSF can be obtained for snRNA-seq by either cell processing strategy.

Neutrophil diversity in the ventricular CSF

Next, we sought to characterize leukocyte populations in greater detail. Re-integration of the 6,017 nuclei identified as neutrophils revealed eight transcriptionally-distinct neutrophil sub-clusters. All eight of these sub-clusters were detected in both preservation methods (**Fig. S2A-D**), but with varying proportions. We annotated these neutrophil sub-clusters via comparisons to scRNA-seq of neutrophil states in the blood and in lumbar CSF[16], enabling us to merge the eight sub-clusters into three broad neutrophil populations (**Fig. 3A, Table S4**). The majority of neutrophils form a continuum from Nascent Neutrophils (21.29%) (neu4, neu6, neu8), which expressed *S100A8*, *S100A9*, and *SELL*, to Quiescent Neutrophil states (65.43%) (neu1, neu2, neu5, and neu7), which expressed markers such as *MALAT1* and *CXCL8* (**Table S2**). In addition, a third population expressed genes that are activated during interferon (IFN) responses (13.28%) (neu3), including *IFIT1*, *IFIT2*, *IFIT3*, and *FCGR3B*. These IFN-Activated Neutrophils are a cell population with diverse but not fully characterized functions[17,18]. To our knowledge, they have never been described in the CSF previously.

To further characterize these neutrophil populations, we scored them on the activity of marker genes for neutrophil populations identified in the blood in two previous scRNA-seq studies by Wigerblad et al.[16] (**Fig. 3B, Tables S3, S8**) and Kwok et al.[19] (**Fig. S3A, Tables S3, S8**). We also scored neutrophils for the activity of 12 gene co-expression modules (N1-N12) computed within the neutrophils from our snRNA-seq data to describe distinct patterns of activity across the neutrophil populations (**Fig. 3C, S4A Table S4**).

Nascent Neutrophils were defined by elevated expression of markers for the "Nh0" immature neutrophil population from the Wigerblad dataset (adjusted $p = 2.86\times10^{-153}$), as well as markers for two immature neutrophil populations from the Kwok dataset (S100A8-9 hi neutrophil markers (adjusted $p = 6.10\times10^{-219}$) and IL1R2^{+} immature neutrophil markers (adjusted $p = 2.55\times10^{108}$). Nascent Neutrophils also displayed high expression of gene co-expression module N7 (adjusted $p = 7.27\times10^{-99}$). Genes in this module were over-represented for NF-κB activation genes (GO:0051092) and signaling pathways for pattern recognition protein receptors (GO:0002221), Toll-Like receptors (GO:0002224), and cytokine receptors (GO:0019221, GO:0004896), including cytokine-signaling pathways related to IL-12 (GO:0032655), and IL-1 (GO:0032651, GO:0005149).

Quiescent Neutrophils were defined by the expression of long noncoding RNAs that modulate with inflammatory responses (e.g., *MALAT1*, *NEAT1*, and *LUCAT1*[20–23]) and genes that are associated with neutrophil migration and chemotaxis (e.g., *SSH2*, *DOCK5*, *CXCL8*[24–26]). While markers of the Wigerblad 'Nh2' "transcriptionally inactive" cluster had overall low expression in our dataset, Quiescent Neutrophils had a modestly increased expression of these markers relative to the other neutrophil populations ($\log_2FC = 0.190$, adjusted $p = 4.94\times10^{-37}$). Several gene co-expression modules were upregulated in Quiescent Neutrophils, including N5 (adjusted $p = 3.02\times10^{-16}$), N3 (adjusted $p = 1.61\times10^{-39}$), N10 (adjusted $p = 1.24\times10^{-27}$), and N11 (adjusted $p = 1.88\times10^{-64}$). *MALAT1* and *NEAT1* were members of N5, suggesting a role for this module in the epigenetic regulation of inflammatory responses. N5, N3, and N11 were over-represented in genes associated with serine/threonine kinase activity (GO:0004674), with the strongest upregulation of *SIK3*, *STK4*, and *CAMK1D*. Serine/threonine kinases, including *STK4* and *CAMK1D*, have been reported to play a variety of roles in neutrophils[27–29], but their

160 functional significance in the Quiescent Neutrophil population is unclear. Interestingly, *CAMK1D* and *MALAT1*
161 have also been found to be co-expressed in a subset of granulocytes in the blood[30].
162
163 The neutrophil module N12 consists of several genes that play roles in cell adhesion and migration (ADGRG3,
164 ADGRE2, MYADM, ADAM8). The elevated expression of this module in nascent (adjusted $p = 5.03\times10^{-74}$) and
165 quiescent neutrophils (adjusted $p = 9.55\times10^{-06}$) may suggest an active recruitment of these cells at the time of
166 sample collection.
167
168 IFN-Activated Neutrophils were defined by elevated expression of many canonical interferon-stimulated genes,
169 genes. Markers of the 'Nh3' "IFN inducible" neutrophil population in the Wigerblad dataset were strongly induced
170 (adjusted $p < 2.23\times10^{-308}$), as was gene co-expression module N8 (adjusted $p = 1.31\times10^{-269}$), whose hub genes
171 included canonical interferon-stimulated genes such as *IFI6, IFI30, IFI44*, *IFI44L, IFIT1, IFIT2* and *IFIT3*. Other
172 marker genes annotated as activated in response to symbionts (GO:0140546), viruses (GO:0051607), cytokines
173 (GO:0034097), and interferons (GO:0034341, GO:0034340, GO:0035456) included *MX1, IFITM3, IFIT5, IFI6,*
174 *CD74, CXCR4, and SELL*. This cell state also had decreased expression of the *IL1B*-containing module N10
175 (adjusted $p = 1.24\times10^{-63}$), consistent with the suppressive effects of interferons on IL-1 production[31].
176
177 ***Monocyte/Macrophage diversity in the ventricular CSF***
178 We performed similar analyses to characterize monocyte lineages in ventricular CSF (**Fig. 4**). By sub-clustering
179 the 2,920 monocyte-lineage cells, we identified 6 transcriptionally distinct Seurat clusters annotated based on
180 gene expression markers in the literature as classical monocytes (four clusters, 90.6%), macrophages (5.2%),
181 and dendritic cells (4.2%) (**Fig. 4A, Fig. S5A-D, Table S5**). We further characterized these clusters of
182 monocytes/macrophages based on comparison to publicly available gene expression data for monocyte clusters
183 in the MoMac data set[32], which integrated monocytes in health and disease states from 41 studies in 13 different
184 tissues (**Fig. 4B, Fig. S6A, Table S6**). We also performed genes co-expression module detection and obtained
185 11 transcriptionally distinct modules (M1-M11), which helped us better define the cell states we observed (**Fig.**
186 **4C, Fig. S7A, Table S7**).

187

188 Classical monocyte markers (*SELL, CSF1R, ITGAX, CD163, CSF3R, S100A8*, *S100A9*, *S100A12, ALOX5AP*)
189 were split between four distinct clusters that also expressed markers associated with monocyte activated or
190 inflammatory states (*HLA-DRA, HLA-DRB1, CD163, IL1B, CXCL8, CCL3, CCL4, CXCL5,* members of the TNF
191 family); hence we have labelled them Activated Classical Monocytes (AC Mono). We defined each of the four
192 AC Mono subtypes by its most differentially expressed genes encoding secreted proteins: ACMono-VCAN
193 (36.68% of all monocyte/macrophage cells), ACMono-PROK2 (36.1%), ACMono-CXCL8 (15.24%), and
194 ACMono-CXCL5 (2.53%). The first two subtypes were the most abundant and had in common a pro-
195 inflammatory signature including interferon-induced genes, while the latter two were defined by their high
196 expression of neutrophil-attracting chemokines.

197

198 ACMono-VCAN was the most abundant monocyte subtype. Its eponymous marker *VCAN* (avg $\log_2$FC = 2.64,
199 adjusted p = 1.53×10^{-268}), encodes versican, a chondroitin sulfate proteoglycan that modulates inflammatory
200 responses in many cell types[33,34]. It has been reported that *VCAN* activation in monocytes/macrophages is
201 dependent on Type I interferon signaling[35]. Consistent with this, we observed elevated expression of the
202 interferon-induced genes *IFI44* and *IFI44L.* ACMono-VCAN also had upregulation of genes in co-expression
203 modules M2 (adjusted p = 1.35×10^{-118}) and M3 (adjusted p = 1.05×10^{-113}), enriched for viral defense responses
204 and endocytic/phagocytic genes, respectively (**Table S7**). For instance, scavenger protein genes such as *STAB1*
205 (avg $\log_2$FC = 1.83, adjusted p = 1.18×10^{-117}) and *CD163* (avg $\log_2$FC = 1.76, adjusted p = 2.25×10^{-83}) were
206 upregulated, along with components of the THBS pathway (**Fig. 5C**), suggesting that this is an interferon-
207 activated cell state responding through modification of the cell matrix. By contrast, ACMono-VCAN appeared not
208 to be activated by other cytokines such as interleukin-1, as it had decreased expression of M5 (adjusted p =
209 7.42×10^{-164}), a gene co-expression module enriched in genes involved in cellular response to interleukin 1
210 (GO:0071347), apoptotic process (GO:0006915), and NF-κB signaling (GO:0007249) module.

211

212 ACMono-PROK2 was characterized by the expression of *PROK2* (avg $\log_2$FC = 1.76, adjusted p = 1.68×10^{-38}),
213 encoding prokineticin-2, a peptide with chemokine–like activity that is highly expressed in many classical
214 monocytes[36] with roles in cell migration[37,38] and differentiation[39,40] and neurogenesis[41,42]. More broadly, the

ACMono-PROK2 gene signature suggests a pro-inflammatory state, with elevated expression of gene co-expression module M8 (adjusted $p = 3.52\times10^{-115}$), including the cytokines *TNF*, *IL6*, and *IL1B*, and genes related to NF-κB signaling. Comparisons to MoMac revealed overlap with MoMac clusters 1 (adjusted $p = 2.35\times10^{-126}$) and 8 (adjusted $p = 4.13\times10^{-101}$), both of which are subtypes of $CD16^{+}$ monocytes with high expression of inflammatory genes.

ACMono-CXCL8 was defined by elevated expression of pro-inflammatory ligands such as *CXCL8*, *CCL3*, and *CCL4*, markers of activated M1-like monocytes that act as chemoattractants for other monocytes, neutrophils, NK cells, and T-cells[43]. ACMono-CXCL8 had high expression of markers for Module M5 (adjusted $p = 1.60\times10^{-142}$), which was enriched for Gene Ontology terms related to vesicle secretion (e.g., Proton-Transporting V-type ATPase (GO:0033180), positive regulation of exosomal secretion (GO:1903543), and multivesicular body secretion (GO:0032585) and with the interleukin-1-mediated signaling pathway (GO:0070498). Similarly, ACMono-CXCL8 had elevated expression of Module M9 (adjusted $p = 6.07\times10^{-101}$), which consists primarily of genes associated with vesicle production. This cluster also highly expressed markers of the “IL1B” MoMac Cluster 15 (adjusted $p = 2.30\times10^{-141}$), as well as the NF-κB transcription factor inhibitor *NFKBIA,* which regulates the pro-inflammatory activities of NF-κB downstream of TLR4. Collectively, these enrichments suggest that ACMono-CXCL8 may have M1-like activity.

ACMono-CXCL5, the smallest monocyte population, expressed activated monocyte ligands such as *CXCL5* and *CXCL3* that are known for their roles as chemoattractants for myeloid cells. In common with ACMono-CXCL8, ACMono-CXCL5 had elevated expression Module M9 (adjusted $p = 2.85\times10^{-6}$), and MoMac Cluster 15 (adjusted $p = 2.95\times10^{-12}$).

Macrophages (Mac) represented 5.24% of cells in the monocyte lineage. In addition to genes that are largely expressed in macrophages such as *GPNMB, PLD3* and *CTSD*, these cells were marked by high expression of pro-inflammatory genes such as *HIF1A-AS3*[44] *FTL*[45], and *MDM2*[46]. *FTL* expression in macrophages has been associated with exposure to oxidized low-density lipoprotein[47]. Consistent with this, we found high expression of

242 several genes associated with lipid-associated macrophages (e.g., *CSTB*, *CTSD*, *GPNMB*, *LGALS3*, *PLD3*, and
243 *PLIN2*[48]), which are also induced in macrophages in a murine model of stroke[49]. Interestingly, we also detected
244 high expression for markers of MoMac cluster 3 (adjusted $p = 1.50\times10^{-26}$), a TREM2^{+}, M2-like population. Overall,
245 these annotations demonstrate the presence of macrophages in the CSF after IVH and provide evidence for
246 heterogeneous reactive states.

247

248 The final sub-population (4.21%) expressed markers of dendritic cells (DC). We annotated these cells as DC
249 based on shared markers with MoMac cluster 14 (adjusted $p = 5.54\times10^{-22}$), described by the MoMac authors as
250 dendritic cell contamination. We note, however, that dendritic cells share several markers with intermediate
251 monocytes, making a definitive annotation difficult. Some cells in the cluster expressed intermediate monocyte
252 markers such as *CIITA*, suggesting a mixed population (**Fig. S5D)**. Notably, this population was also
253 distinguished by elevated expression of MHC class II markers such as *HLA-DRA, HLA-DRB1, HLA-DQA1 and*
254 *HLA-DQA2*, suggesting that these cells may have the ability to interact with and activate CD4^{+} T cells.

255

256 ***Lymphocyte diversity in the intraventricular CSF***

257 The 1,990 nuclei identified in our data as lymphocytes expressed canonical pan-lymphocyte and T cell markers,
258 such as *PDE3B*, *FOXP1*, *MBNL1*, *ANK3*, *BCL2*, *FYN*, *SKAP1* and *CD247*. A small population of these cells
259 expressed B-cell markers (*CD19*, *CD20*, *CD21*), consistent with observations for intraparenchymal hematoma
260 and CSF in subarachnoid hemorrhage by flow cytometry[15,50]. *De novo* clustering of lymphocytes did not clearly
261 define known T- or B-cell subtypes, most likely because of the relatively small number of cells representing each
262 subtype. Therefore, to better characterize lymphocyte populations, we performed a label transfer analysis by
263 integrating our lymphocytes with those from a large PBMC reference atlas and projected our data onto the UMAP
264 from the reference data to identify shared marker genes and confirm annotations[51] (**Fig. 5**). This analysis
265 suggested that most of the lymphocytes we detected were CD4^{+} subtypes, especially central memory T-cells
266 (28.5%) and CD4^{+} naïve T-cells (41.6%). CD8^{+} effector memory T-cells represented an additional 14.7% of
267 lymphocytes. Double-negative CD4^{-}CD8^{-} T-cells represented 10.4% of all lymphocytes, suggesting an

268 enrichment of activate T-cell states. Consistent with this, further sub-clustering revealed a population expressing
269 pro-inflammatory markers such as *S100A8*, *S100A9*, *CSF3R*, *IFITM2*, and *CXCR2*, a marker of γδ T-cells[52].

270

271 ***Intercellular communication networks in the intraventricular CSF***

272 Chemokine ligands and their receptors were markers for several sub-populations of neutrophils, monocytes, and
273 lymphocytes. For instance, the chemokine *CXCL8* was expressed almost exclusively by ACMono-CXCL8, while
274 its receptor, CXCR2, was expressed primarily by neutrophils. The specific expression of these ligand-receptor
275 pairs provides the potential for signaling between populations. To more rigorously investigate this putative cell-
276 cell communication, we made use of Immune Dictionary[53] and the CellChat[54,55] package in R.

277

278 The Immune Dictionary provides single-cell transcriptomic profiles of 17 immune cell types in response to
279 treatment with each of 86 cytokines in mice. We reasoned that similarities between cells in our data set and
280 those responsive to specific cytokines in the Immune Dictionary imply common stimuli. We observed expression
281 of IL-1α-induced genes in all three neutrophil populations (**Fig. 6A, Table S8**). In the IFN-activated neutrophil
282 population, expression signatures of interferon responses (Type I and Type II) and IL-1 signaling (IL-1α, IL-1β,
283 IL-15, IL-18, and IL-36α) were evident. While IFN-activated neutrophils were IL-1 responsive, they were not IL-
284 1 productive, as they were negatively associated with co-expression module N10, a hub gene of which was *IL1B*.
285 This is consistent with observations that Type I interferon can suppress IL-1 production[31]. In contrast, monocytes
286 generally showed a greater expression of genes that are suppressed by IFN-α1 and IFN-γ stimulation (**Fig. S8**
287 **A-D**). Monocytes also expressed IL-1α- and IL-1β induced genes at high levels. Interestingly, PROK2 monocytes
288 expressed higher levels of genes that were both induced and suppressed by IL-1α and IL-1β, suggesting a
289 complex remodeling of the IL-1-modulated transcriptome. ACMono-VCAN, ACMono-CXCL5, and DC cells
290 expressed a signature observed in monocytes treated with IL-33 (**Fig. 6B**), which is an IL-1 family cytokine that
291 is released in response to cell stress or damage. Macrophages shared with monocytes an IFN-α1 and IFN-γ
292 suppressed expression profile, but also highly expressed genes that were suppressed by IL-1α.
293 We further delineated intercellular communication networks using CellChat, which uses the expression patterns
294 of receptor-ligand pairs to identify cell types with the potential for cell-cell communication. Doing so, we found
295 that the expression of ELR-motif CXC chemokines linked ACMono-CXCL5 and ACMono-CXCL8 to chemokine

296 receptor CXCR1- and CXCR2-expressing neutrophils. This pathway is particularly important for neutrophil
297 recruitment and activation, suggesting a role for macrophages in facilitating this function. In addition, ACMono-
298 CXCL8 contribute CC chemokines that tie them to IFN-activated neutrophils specifically. CellChat also revealed
299 interactions between subtypes of neutrophils, mediated by ADGRE and SELPLG/SELL. Other interactions are
300 shown in **Fig. 6C and 6D**.
301
302 Integrating observations from Immune Dictionary and CellChat suggested complex behaviors not evident from
303 either data set alone. For example, from Immune Dictionary we observed that ACMono-CXCL5 shared common
304 gene expression features with macrophages stimulated by the IL-1 family cytokine IL-33. CellChat indicated that
305 ACMono-CXCL5 also contribute IL-1, suggesting an IL-1 signaling positive feedback loop in this macrophage
306 subtype.
307
308 ***Development of a flow cytometry panel for neutrophil and monocyte diversity in the ventricular CSF***
309 Our snRNA-seq data suggest that specific immune cell subtypes are enriched in the CSF of IVH patients
310 compared to their prevalence in other contexts. Monitoring the abundance and dynamics of these immune cell
311 subtypes could potentially reveal biomarkers that predict clinical outcomes. However, snRNA-seq is not a
312 practical method to track these populations in clinical settings. Leveraging our snRNA-seq data, we sought to
313 develop a panel of cell surface markers to distinguish neutrophil and monocyte subtypes by flow cytometry.
314
315 We therefore developed a flow cytometry panel to delineate functional states of neutrophils and monocytes, the
316 two most common cell types observed in our snRNA-seq data. To leverage the insights of our snRNA-seq data,
317 we derived this panel empirically from our data set, as opposed to relying on existing cytometry-based
318 classifications. After identifying cluster of differentiation (CD) genes enriched in specific clusters, we used
319 FluoroFinder (Broomfield, CO) to select a subset of markers for which reliable antibodies with compatible
320 fluorophores existed.
321

322 Using this panel, we performed flow cytometry analysis of CSF samples on three samples from two participants
323 with IVH not included in the snRNA-seq analysis. Both participants had experienced thalamic ICH with IVH, one
324 as a result of hypertension and other as a result of a ruptured arteriovenous malformation. As expected, CD45+
325 immune cells could be distinguished as granulocyte, monocyte, and lymphocyte populations using CD3 and
326 CD14 gating, which were further confirmed by forward and side scatter profiles (**Figure 6A**). Based on neutrophil
327 clustering from our snRNA-seq data, we hypothesized that three canonical neutrophil surface markers (CD10,
328 CD62L, and CD16b) could help resolve distinct neutrophil subsets[56]. The dominant population (>90% of
329 neutrophils) was $CD10^{+}CD62L^{+}CD16b^{high}$, consistent with mature circulating neutrophils.

330

331 CD10 presented a particular interpretive challenge: while transcriptional data, including our own and that from
332 Wigerblad et al.[16], suggest CD10 as a marker of nascent neutrophils, it is better established as a surface protein
333 associated with mature neutrophils. Consistent with this, we observed a small population of $CD10^{-}$
334 $CD62L^{+}CD16b^{high}$ neutrophils (<2%) consistent with a nascent phenotype, but no $CD10^{+}CD62L^{+}CD16b^{high}$, as
335 otherwise might have been predicted directly from our transcriptomic data **(Figure 6B)**. From our transcriptomic
336 data, we would infer that quiescent neutrophils are $CD10^{-}CD62L^{-}CD16b^{low}$. However, we again anticipated that
337 the protein-level expression of CD10 would differ for these cells, and that quiescent cells should be $CD10^{+}CD62L^{-}$
338 $CD16b^{low}$. Though both populations are small, the $CD10^{+}CD62L^{-}$ $CD16b^{low}$ population is much more common in
339 our flow cytometry data than is the $CD10^{-}CD62L^{-}$ $CD16b^{low}$ population **(Figure 6B).** A distinct subset of a $CD10^{-}$
340 $CD62L^{-}$ population is $CD10^{-}CD62L^{-}$ $CD16b^{high}$. Cross-referencing with our snRNA-seq data, this population is
341 most consistent with interferon-activated neutrophils, though the markers shown here do not directly test for that
342 state. Additionally, we identified by flow cytometry a $CD10^{+}CD62L^{-}CD16b^{+}$ subset not resolved in our snRNA-
343 seq clustering analysis but reported in the literature as T cell–suppressive neutrophils[57]. Similarly, we
344 hypothesized that monocyte subtypes could be distinguished using the markers CD163, CD62L, CXCR1,
345 CXCR2, CD50, and CD87. We found that of these, CD163, CD62L, and CXCR1 were the only markers with
346 discriminating power in our flow cytometry data set (**Figure 6C**).

347

348 We note that we detected nascent, quiescent, and interferon-activated populations — which together dominate
349 the snRNA-seq neutrophil profile -- at very low levels in our flow cytometry data. It is unclear whether this arises
350 from greater sensitivity of snRNA-seq; misclassification by snRNA-seq due to mismatch between gene and
351 protein expression; limitations of the flow cytometry panel; or patient-specific differences in neutrophil subtype.
352 Taken together, however, our flow cytometry results indicate that it may be possible to translate leukocyte
353 functional states inferred from single-nucleus transcriptomics into clinically-feasible flow cytometry panels.

354

355 **Discussion**

356 In this study, we generated a single-nucleus transcriptomic atlas of the ventricular CSF in IVH. We leveraged
357 nuclear extraction as a strategy to enrich for cell types — specifically neutrophils — that are often challenging to
358 capture in single-cell experiments because of their fragility. Our results revealed a diversity of cell types, including
359 distinct subpopulations of neutrophils, monocytes, and lymphocytes. Notably, we captured a large and diverse
360 population of neutrophils, including a population of interferon-activated neutrophils that has not been described
361 in the central nervous system previously. As single-nucleus RNA sequencing is not feasible for clinical diagnostic
362 purposes, we validated potential flow cytometry markers for cellular sub-clusters we identified. This
363 demonstrates the feasibility of translating biomarkers derived from snRNA-seq data into clinically practical flow
364 cytometry markers.

365

366 A strength of our study that distinguishes it from previous studies is the detection of a large population of
367 neutrophils in the CSF. Neutrophils are expected to be among the most common leukocytes present in the CSF
368 during the first several days after hemorrhage[58]. Neutrophil depletion has been shown to be protective in a range
369 of hemorrhagic brain disease models[59–61]. Yet previous sequencing studies in these diseases have selected
370 against neutrophils in sample processing. Sansing and colleagues reported single-cell RNA sequencing data
371 from the intraparenchymal hematoma of a patient who underwent clot evacuation after an intracerebral
372 hemorrhage as part of the MISTIE III phase III clinical trial[62] and have recently extended this work to a larger
373 group of subjects undergoing clot evacuation[63]. Their study provides a rich time-dependent atlas of leukocytes
374 in the intracerebral hematoma, but only a small population of neutrophils was detected because they subjected

375 samples to a specific granulocyte depletion. Similarly, the two reported single-cell studies of CSF in subarachnoid
376 hemorrhage[64,65] specifically selected against neutrophils, one profiling PBMCs and the other profiling
377 $CD8^{+}CD161^{+}$ cells. Until recently, neutrophils were thought to display a relatively limited functional repertoire,
378 owing to their relatively low transcriptional activity and short lifespans. Single-cell RNA sequencing has revealed
379 that, in fact, neutrophils are highly diverse cell populations[16,66,67,68]. This expanded understanding of the diversity
380 of neutrophils prompted us to investigate this cell population more comprehensively in IVH.
381
382 Neutrophils may be particularly challenging to capture in single-cell studies. They are often short-lived and highly
383 sensitive , rendering them difficult to capture with methods that have long or complex workflows. This raises the
384 question of why we were able to identify a large population of neutrophils when others have not. We analyzed
385 CSF instead of parenchymal hematoma, and these may have different cell populations. However, numerous
386 neutrophils can be isolated from parenchymal hematoma by flow cytometry[69]. It is likely that differences in our
387 sample preparation account for the preservation of neutrophils. The use of single-nucleus instead of single-cell
388 RNA sequencing may improve the identification of neutrophils, as all cells undergo lysis, reducing the bias
389 against fragile neutrophils. While we cannot fully exclude the possibility that the nuclei we identified as deriving
390 from neutrophils actually arise from other cell types, the expression of canonical neutrophil markers in these cells
391 supports their assignment.
392
393 A strength of single-nucleus RNA sequencing over traditional cytometric approaches is the ability to distinguish
394 subtle cellular phenotypes and activation states. The advent of these methods has revealed that neutrophils,
395 previously thought to be a relatively homogenous cell type, in actuality exhibit a variety of states[16]. In this case,
396 we identified three major neutrophil functional states, though we anticipate that with larger sample sizes and
397 improved isolation techniques, it is likely we would be able to classify these states even more specifically. We
398 have shown that these are consistent with classifications of neutrophils derived from peripheral blood in
399 independent data sets[16,19].
400
401 One particularly interesting neutrophil state is the IFN-activated neutrophil. To our knowledge, this subtype of
402 neutrophils has not been reported in the human central nervous system previously, though it has been detected

403 in rodents[70]. Interferons have been known to stimulate neutrophils for nearly half a century[71]. It was recently
404 reported that interferon-activated neutrophils play an important role in tumor control[17,72] and the response to
405 SARS-CoV-2 infection[18]. Knockout of the Type I interferon receptor results in increased neutrophil accumulation
406 in infected tissue[73,74], while interferon-gamma decreases neutrophil accumulation in such tissue[75]. Our analysis
407 based on Immune Dictionary suggests that Type I and II responses may be particularly relevant to IFN-activated
408 neutrophils in IVH.
409

410 A study of soluble factors in the CSF after IVH identified time-dependent increases in the Type II interferon IFN-
411 γ that were augmented in patients treated with intraventricular tissue plasminogen activator; no subjects in our
412 study underwent such treatment[76]. Similarly, IFN-γ levels in the CSF were associated with white matter damage
413 in premature infants with posthemorrhagic hydrocephalus[77]. Little is known about the role of Type I interferons
414 in human IVH, though a nonsense single-nucleotide polymorphism in the gene encoding IFN-ε is associated with
415 the development of ICH[78]. In a rat germinal matrix hemorrhage model, treatment with Rh-IFN-α improved
416 neurological function[79]. Our findings suggest that the Type I interferon response in general, and interferon-
417 activated neutrophils in specific, merit further investigation in the pathophysiology of intraventricular hemorrhage.
418 This represents a potentially targetable pathway for modulating neutrophils for future therapies.
419

420 Our data also reflect a diversity of monocytes/macrophages that occupy a range of functional states. These
421 states corresponded to strong differential expression of genes encoding certain secreted proteins, which may
422 give some indication to their role in IVH and other acute brain injuries. The distinction we observed between
423 macrophages expressing lipid metabolism genes and monocytes expressing cytokine-stimulated genes was
424 previously noted for tumor-associated cells[32]. We further classified monocytes into four activated states
425 defined by their expression of genes encoding specific secretory proteins. *VCAN ACMono* and *PROK2*
426 *ACMono* exhibited transcriptomic profiles that could be described broadly as pro-inflammatory and interferon-
427 responsive, gene co-expression network analysis revealed markedly different profiles for these cellular states.
428 Increased deposition of versican (encoded by *VCAN*), a protein that is involved in myelination, has been noted
429 in the brains of rabbit pups subjected to IVH[80]. Overexpression of *PROK2* has been shown to reduce
430 neurodegeneration and functional deficits in a mouse model of TBI[81]. Both the VCAN ACMono and PROK2

431 ACMono express interferon-response genes, again supporting an outsize role of interferon signaling in the
432 immune response to IVH. Further insight can be gleaned receptor-ligand interactions, such as CXCL8 and
433 CXCR2, which we have characterized more extensively using CellChat. These results indicate cross-talk within
434 subtypes of individual cell types (e.g., PROK2 with CXCL8 ACMono) or between cell types (e.g., PROK2
435 ACMono with IFN-activated neutrophils). Major roles for the ELR-motif CXC chemokines, CC chemokines, IL-1
436 family cytokines, and interferons were observed. We also observed monocyte/macrophage phenotypes that
437 have been associated with disease. For example, both snRNA-seq and flow cytometry revealed a substantial
438 number of $CD163^+$ monocytes/macrophages, a population that has been associated with disease severity in
439 aneurysmal subarachnoid hemorrhage[82].
440
441 The distribution of lymphocytes we observed in the CSF is intriguing and merits further investigation. The majority
442 of cells were $CD4^+$ T cells. It has been reported that the majority of T cells in the CSF under normal conditions
443 exhibit a central memory phenotype[83]. This was one of the major subtypes we observed in IVH, though not the
444 most common. These cells have been purported to enter the CSF via the choroid plexus[84].
445
446 Limitations of our study include a small sample size and insufficient material for genotyping, both of which reduce
447 our ability to delineate differences inflammatory profiles that are associated with disease severity. These samples
448 were convenience samples that were obtained when specific clinical events (EVD placement, EVD removal, or
449 diagnostic testing) prompted CSF sampling, increasing the heterogeneity of the samples and potentially creating
450 sampling bias. In addition, low cell counts from individual subjects further limit the generalizability of our results.
451 Nevertheless, our study is one of very few single-cell or single-nucleus transcriptomic studies of cerebrospinal
452 fluid for hemorrhagic brain disease, and substantially increases the data available in the literature. While we
453 hypothesize that the single-nucleus approach has allowed us to capture difficult-to-detect neutrophil states, this
454 approach does have drawbacks. Nuclei contain substantially fewer transcripts than do whole cells, potentially
455 diminishing our ability to identify transcriptionally regulated pathways relevant to disease biology. Nevertheless,
456 even small nuclear transcriptomes have proven reliable for cell type classification in our study. While single-cell
457 transcriptomic methods are unlikely to be translatable directly to clinical diagnostics, they may generate

458 candidates for the development of flow cytometry panels. We provide a proof-of-concept for this here, but with
459 too few subjects to demonstrate the utility of these markers for diagnostic or prognostic purposes.

460

461 It would be valuable to extend our approaches to elucidate time-dependent changes in blood and CSF leukocytes
462 across a larger cohort of patients in ICH, SAH, IVH, and TBI. Previous studies report divergence in leukocytes
463 sampled from the blood and central nervous system over time[15,62]. The distinct immune profile in the CSF and
464 brain after IVH may yield insights into the risk for common complications, such as persistent hydrocephalus.
465 Such information could help to inform the timing of surgical interventions and reveal strategies to guide treatment
466 of post-hemorrhagic hydrocephalus.

467

468 Taken together, our results provide the most comprehensive cellular atlas of the CSF in IVH to date. This atlas
469 reveals a rich diversity of cellular populations, including myeloid states not previously described in the human
470 central nervous system, including interferon-responsive neutrophils. We have further demonstrated that
471 transcriptional markers from these populations can in many cases be validated at a protein level with flow
472 cytometry. We anticipate that these results will set the stage for larger studies that elucidate the relevance of
473 specific leukocyte subtypes to disease severity, progression, and outcome. Eventually, this will yield new
474 diagnostic tools and therapeutic targets for intraventricular hemorrhage, a common, catastrophic disease with
475 few effective treatments.

476

477 **Materials and Methods**

478 *Sex as a biological variable*

479 As we collected convenience samples and batched nuclei for sequencing (see below), we were unable to
480 interrogate sex as a biological variable specifically; N=6 samples were from male subjects and N=1 sample was
481 from a female subject. For the period of enrollment, a recruitment flow chart is shown in **Figure S9**.

482 *Statistics*

483 Statistical methods used in this study are described in the sections pertaining to each specific assay or analytical
484 tool.

485 *Study approval*

486 Subjects (N=7; ICH=6, SAH=1) are a subset of those included in a prospective cohort study of patients aged 18-
487 88 with potentially life-threatening neurologic illness (*NCT04189471*). The University of Maryland, Baltimore,
488 institutional review board (IRB) approved this study, entitled "Improving Outcomes for Patients with Life-
489 Threatening Neurologic Illnesses," approval: number HP-00056063, date: August 1, 2013. Written informed
490 consent was obtained from subjects (if they had decision-making capacity) or their legally authorized
491 representatives. Study procedures were performed in accordance with the ethical standards of the responsible
492 committee on human experimentation and with the Helsinki Declaration of 1975. Detailed clinical characteristics
493 of study participants were recorded in a secure database, including Cytospin cytology and computed tomography
494 (CT) scans obtained from the participants as part of the standard of care.

495 *Sample preparation and single-nucleus RNA sequencing.*

496 Of the CSF aspirated from the proximal port of the EVD during routine clinical practice, excess sample was
497 obtained and transported to the laboratory for immediate processing. Obtained CSF was collected on EDTA
498 (purple top vacutainers), with a processing time <1 hour from the time of collection. RNAse and
499 Proteinase/phosphatase were inhibited by adding 1uM DEPC (Sigma D5758) and 1XHALT (Invitrogen 1861281).
500 The cellular component of CSF was obtained by spinning the sample at 350g for 10 min. The pellet was
501 resuspended, and red blood cells were depleted using EasySep magnetic beads (StemCell Technologies
502 cat18170), and Miltenyi microcolumns (Miltenyi cat130-042-701). Samples were then washed and stored at -
503 80C. Half of the samples were stored as pellets and half in cryopreservation media (Cryostor, StemCell
504 Technologies cat 100-1061). All the samples were stored at -80°C for <3 months. For pelleted samples, nuclei
505 extraction was performed directly from the pellets. For samples stored in cryopreservation media, nuclei isolation
506 was performed on the cellular fraction after washing with PBS+1% BSA at 350g/5 minutes at 4C. Nuclei isolation
507 was performed using a detergent-free nuclei isolation kit, Invent (cat IN-024), according to the manufacturer's
508 instructions. Briefly, nuclei were resuspended in buffer A, then vortexed for 20s at level 9 on Genie2 Vortex, then
509 placed on the spin column at 16000g/30s. The pass-through was washed with buffer B and counted on a

510 MoxiGoII (Orflo) using 1uM Propidium Iodide (Sigma P-4864). We loaded two pools, one pool containing
511 samples stored as pellets and other with cellular fraction cryoprotected. A total of 30K isolated nuclei per pool in
512 PBS+1% BSA were loaded in a 10X Chromium X. Sequencing libraries were prepared by the Maryland
513 Genomics core facility at the Institute for Genome Sciences using Chromium Single Cell 3' Kit v3.1 reagents,
514 according to manufacturer's instructions. Libraries were sequenced on a NovaSeq6000 sequencer (Illumina) to
515 an average depth of at least 25,000 raw reads per cell.

516 *Flow cytometry.*

517 CSF samples were acquired from the EVD buretrol chamber. Samples were stabilized in EDTA tubes during
518 transport from the intensive care unit to the laboratory and kept at room temperature. Samples were then spun
519 at 300g for 5 min, at 4ºC. Pellets were then resuspended in 100 µL of staining buffer (phosphate buffered saline
520 with 1% bovine serum albumin and 1% EDTA - A9418 and 324506, Sigma Aldrich), and incubated for ten minutes
521 on ice with Fc Block (ThermoFisher). Pellets were resuspended in 50 µL of staining buffer mixed with antibodies
522 and incubated for an additional 15 minutes in dark. A 13-antibody panel was used for this experiment. Antibodies
523 included mouse anti-human anti-CD45 (363-0459-41, ThermoFisher), mouse anti-human anti-CD3 (344825,
524 BioLegend), mouse anti-human anti-CD14 (367109, BioLegend), human anti-human anti-CD16b (130-123-643,
525 Miltenyi Biotec), mouse anti-human anti-CD163 (333611, BioLegend), human anti-human anti-CD50 (130-115-
526 309, Miltenyi Biotec), mouse anti-human anti-CD183 (353721, BioLegend), goat anti-human anti-CD121a
527 (FAB269F-025, R&D Systems), mouse anti-human anti-CD62L (567989, BD Biosciences), mouse anti-human
528 anti-CD10 (312241, BioLegend), human anti-human anti-CD181 (130-115-950, Miltenyi Biotec), human anti-
529 human anti-CD182 (130-131-233, Miltenyi Biotec), mouse anti-human anti-CD87 (749063, BD Biosciences). 100
530 µL of staining buffer were added, cells were mixed and then spun at 300g for five minutes at 4º C. The supernatant
531 was removed, cells resuspended in 200 µL of staining buffer, and 2 µL of 7-amino-actinomycin D (7-AAD)
532 (420404, BioLegend) were added before flow acquisition. Flow acquisition was performed on a Cytek Aurora 4
533 Spectral Cytometer (Cytek Biosciences, Freemont, CA, USA) (lasers: 355nm, 405nm, 488nm, 640nm) at the
534 University of Maryland Greenebaum Comprehensive Cancer Center Flow Cytometry Shared Service. At least
535 5,000 events were acquired and analyzed with FCS Express V7 software (De Novo Software, Pasadena, CA,
536 USA).

537 *snRNA-seq cell clustering and annotation.*

538 Initial data processing was performed with CellRanger (7.2.0), yielding a cell x gene matrix for each pooled
539 sample. Seurat[51] v4.0.5 was used for batch integration and clustering, using the following parameters. We
540 selected high-quality cells with at least 300 unique molecules and a maximum of 20 percent mitochondrial counts.
541 SCT integration was performed with 5000 variable genes and 20 anchors. Louvain clustering was performed
542 using 20 principal components. An optimal clustering resolution was determined by using the mrtree clustering
543 optimization method[85], which was given resolutions from 0 to 5, with 3.5 (35 clusters) being optimal for the entire
544 population. Cell clusters were annotated to established cell types based on canonical markers from immune cells
545 in other contexts[86–88]. Subsequently, the most abundant major cell types — neutrophils and monocytes — were
546 sub-clustered, following the same procedures starting from the SCT integration step. Cellular populations derived
547 from sub-clustering were compared to neutrophil and monocyte data sets that have been described by scRNA-
548 seq in other contexts[16,19,32]. Cells in our snRNA-seq dataset were scored using the combined expression of
549 marker genes from comparison datasets with the AddModuleScore() function in Seurat. Genes from reference
550 datasets were selected with a $\log_2 FC > 0.585$ (greater than 1.5 fold change) and adjusted p-value < 0.05. We
551 also considered cell annotations derived from label transfer using the Seurat FindTransferAnchors and
552 TransferData functions with 30 principal components and otherwise default parameters. Label transfer was
553 performed separately for monocytes and lymphocytes using level 2 annotations from scRNA-seq of human
554 peripheral blood mononuclear cells[51].

555 *Gene co-expression networks in neutrophils and monocytes.*

556 Gene co-expression modules were identified through k-means clustering of imputed read counts, as previously
557 described[89]. First, we performed a zero-preserving imputation with ALRA[90] to reduce dropouts and improve
558 correlation structure. Next, we performed k-means clustering (parameters). Modules with tightly correlated
559 centroids were merged, and genes with insufficient correlation to the centroids of the merged modules were
560 dropped. These steps were performed using the cells from Pool 2, then projected onto the cells from Pool 1.
561 This strategy reduces the potential for batch effects and provided an independent test set to evaluate the
562 robustness of the modules. Gene Ontology annotations for the modules were obtained using the enrichR
563 package in R from the GO Molecular Function 2023, GO Cellular Component 2023 and GO Biological Process
564 2023 databases.

565 *Cell-cell signaling networks*

566 Cytokine signaling activity among cell types was predicted by two methods: We used the CellChat[54] (v 2.2.0)
567 package in R to predict the incoming and outgoing signals and the associated pathways for each cell type. Cell
568 populations with fewer than 50 cells were excluded due to insufficient data. Incoming) cytokine responses were
569 further evaluated by scoring each cell (for the activity of signatures defined by the set of genes up- or down-
570 regulated (FDR < 0.05) in immune cell populations after exposure to each of 86 cytokines[53]. As the Immune
571 Dictionary was generated in mice, our analysis used human genes with one-to-one orthology. Scores were
572 calculated with Seurat AddModuleScore() for each cytokine / cell type condition in which at least ten differentially
573 expressed genes were detected.

574 *Data availability*

575 We have made our expression data available on the Neuroscience Multi-Omic Analytics (NeMO) platform[91]
576 (https://nemoanalytics.org/p?s=c4d7a449) to facilitate secondary data visualization and analysis.
577 Sequencing data will be available on dbGaP (pending). Code generated for this study is available at
578 https://github.com/Ciryam-Lab/vCSF-Hemorrhage.git.

579

580 **Figure Legends**

581 **Figure 1. Clinical characteristics of study participants.** A. Study design (Created in
582 https://BioRender.com). B. Computed tomography (CT) scans. Axial images (slice thickness=3 mm) from the
583 first CT study obtained after EVD placement for a subject with ICH (i,ii) and SAH (iii, iv). i. Thalamic ICH with IVH
584 most prominent in right lateral ventricle (RLV) and ventriculomegaly consistent with hydrocephalus (HC), with
585 EVD visible in left lateral ventricle. ii. More caudal slice from same CT as in (i) showing IVH in the third ventricle
586 (3V) and bilateral lateral ventricles (LVs). iii. Aneurysmal SAH with small amount of IVH in bilateral LVs, with
587 EVD visible at the foramen of Monro. iv. More caudal slice from same CT as in (iii) showing blood in the basal
588 cisterns in classical aneurysmal SAH pattern, with dilated temporal horns consistent with HC. C. Cell proportions
589 in ventricular CSF assessed by cytospin columns.

590 **Figure 2. snRNA-seq of ventricular CSF after IVH.** A. Uniform manifold approximation and projection (UMAP)
591 plot for snRNA-seq of ventricular CSF (11,191 nuclei from seven study participants). B. Quality metrics
592 comparing cell processing methods. C. Dot plot showing expression of canonical marker genes across cell types.

593 **Figure 3. Neutrophil diversity in CSF after IVH.** A. UMAP indicating neutrophil subtypes. B. Annotation of
594 neutrophil subtypes by scoring with marker genes from neutrophil subtypes identified in the blood[16]. C. Gene co-
595 expression modules differentially expressed across neutrophil subtypes. Wilcoxon rank-sum test (one-sided for
596 reference marker scoring, two-sided for gene co-expression networks) with Bonferroni correction used for
597 statistical significance testing (see Tables S3, S4). *$p < 0.05$, **$p < 0.01$, ***$p < 0.001$, ****$p < 0.0001$.

598 **Figure 4. Monocyte diversity in CSF after IVH.** A. UMAP indicating monocyte subtypes. B. Annotation of
599 monocyte subtypes by scoring with marker genes from select subtypes identified in a meta-analysis of
600 monocytes and macrophages from healthy and diseased samples (MoMac)[32]. C. Gene co-expression modules
601 differentially expressed across monocyte subtypes. Wilcoxon rank-sum test (one-sided for reference marker
602 scoring, two-sided for gene co-expression networks) with Bonferroni correction used for statistical significance
603 testing (see Tables S6, S7). *$p < 0.05$, **$p < 0.01$, ***$p < 0.001$, ****$p < 0.0001$.

604 **Figure 5. Lymphocyte diversity in the ventricular CSF.** A. UMAP showing reference annotations in blood
605 from the Azimuth data set[51]. B. Annotation of lymphocyte subtypes in CSF after IVH based on label transfer
606 analysis. (C.,D.) Dot plots showing expression of marker genes in the reference set (C) and our lymphocyte
607 population in CSF after IVH (D).

608 **Figure 6. Intracellular communication in ventricular CSF.** A. Neutrophils in CSF scored by genes upregulated
609 in Neutrophils from the Immune Dictionary upon IFNa1 exposure. B. Monocytes, dendritic cells and
610 macrophages in CSF scored by genes upregulated in Monocytes from the Immune Dictionary upon IL33
611 exposure. C. Circos plot showing strength of outgoing and incoming signals across cell states in the vCSF, based
612 on CellChat analysis. D. Heatmap of outgoing and incoming signal patterns for cytokine classes across all the
613 cell states in the vCSF, based on CellChat analysis.

614 **Figure 7.** Flow cytometry of CSF after IVH. Aggregate data from n=3 samples from n=2 patients is shown, for a
615 total of 72,725 events. A. Gating strategy for identifying the singlet, live, $CD45^+$ cell population (53,424 events)
616 with CD3 and CD14 used to distinguish neutrophils (orange), monocytes (blue), and lymphocytes (green). Back

617 gating onto the SSC-A vs. CD45 plot shows separation of these populations based on the characteristic
618 distribution of these cells types by side scatter. B. Neutrophil population is further gated by CD10 and CD62L.
619 Each quadrant is subsequently gated by either CD16b, CXCR1, or CXCR2. C. Monocyte population is further
620 gated by CD62L and CD163. Each quadrant is subsequently gated by CXCR1.

621

622 **Supplementary Figure S1. UMAPs of ventricular CSF colored by quality metrics.** UMAPs of snRNA-seq of
623 ventricular CSF (11,191 nuclei from seven study participants) colored by A. Preservation method. B. RNA Counts.
624 C. Percentage Mitochondrial Counts.

625 **Supplementary Figure S2. UMAPs of the neutrophil subset colored by quality metrics.** UMAPs of snRNA-
626 seq of the neutrophil subset colored by A. Preservation method. B. RNA Counts. C. Percentage Mitochondrial
627 Counts. D. Dot plot showing marker genes for neutrophil subtypes.

628 **Supplementary Figure S3. Annotation of neutrophil subtypes**. Violin plots of neutrophil subtypes scored by
629 marker genes from cell states found in blood during sepsis response[19].

630 **Supplementary Figure S4. Gene co-expression Modules.** 12 neutrophil gene co-expression modules
631 differentially expressed across neutrophil subtypes.

632 **Supplementary Figure S5. UMAPs of the monocyte subset colored by quality metrics.** UMAPs of snRNA-
633 seq of the monocyte subset colored by A. Preservation method. B. RNA Counts. C. Percentage Mitochondrial
634 Counts. D. Dot plot showing marker genes for monocyte subtypes.

635 **Supplementary Figure S6. Annotation of monocyte subtypes**. Violin plots of monocyte subtypes scored by
636 marker genes from all the cell states found in the MoMac dataset[32].

637 **Supplementary Figure S7. Gene co-expression Modules.** 11 monocyte modules differentially expressed
638 across monocyte subtypes.

639 **Supplementary Figure S8 Cytokine Response Scores.** Heatmap showing of CSF A. neutrophils, B.,
640 monocytes, C. macrophages, and D. dendritic cells showing mean log fold changes of scores based on
641 differential gene expression in response to specific cytokines derived from Immune Dictionary. All interleukin and
642 interferon cytokines eliciting a response in that cell type in Immune Dictionary are plotted.

643

644 **Supplementary Table S1.** Marker genes for all cell types.

645 **Supplementary Table S2.** Marker genes for neutrophil subtypes.

646 **Supplementary Table S3.** Neutrophil subtype marker genes from prior studies and enrichment scores.

647 **Supplementary Table S4.** Neutrophil gene co-expression module membership and functional enrichment.

648 **Supplementary Table S5.** Marker genes for monocyte subtypes.

649 **Supplementary Table S6.** Monocyte subtype marker genes from prior studies and enrichment scores.

650 **Supplementary Table S7.** Monocyte gene co-expression module membership and functional enrichment.

651 **Supplementary Table S8.** Cytokine activity scores using Immune Dictionary signatures and CellChat.

652 **Supplementary Table S9.** Flow chart of subject recruitment.

653 **Acknowledgments**

654 P.C. received funding from the Henry M. Jackson Foundation for the Advancement of Military Medicine,
655 Neurocritical Care Society, and Passano Foundation. P.C. and S.A.A. received funding from the Brain Aneurysm
656 Foundation. S.M. was supported by NIH R01 MH052716. The authors thank Flow Cytometry Shared Service of
657 the University of Maryland Marlene and Stewart Greenebaum Comprehensive Cancer Center. This publication
658 was supported by funds through the Maryland Department of Health's Cigarette Restitution Fund Program – CH-
659 649-CRF and the National Cancer Institute - Cancer Center Support Grant (CCSG) - P30CA134274. Graphical
660 abstract and Figure 1 schematic created in BioRender (https://BioRender.com/q4n1xt9).

661 **References**

662 1. Gaberel, T., Magheru, C. & Emery, E. Management of non-traumatic intraventricular hemorrhage.
663 *Neurosurg Rev* **35**, 485–494; discussion 494-495 (2012).
664 2. Ziai, W. C. *et al*. Occurrence and impact of intracranial pressure elevation during treatment of severe
665 intraventricular hemorrhage. *Crit Care Med* **40**, 1601–1608 (2012).

3. Bhattathiri, P. S., Gregson, B., Prasad, K. S. M., Mendelow, A. D., & STICH Investigators. Intraventricular hemorrhage and hydrocephalus after spontaneous intracerebral hemorrhage: results from the STICH trial. *Acta Neurochir Suppl* **96**, 65–68 (2006).
4. Shah, V. A. *et al.* One-Year Outcome Trajectories and Factors Associated with Functional Recovery Among Survivors of Intracerebral and Intraventricular Hemorrhage With Initial Severe Disability. *JAMA Neurol* **79**, 856–868 (2022).
5. Lovasik, B. P. *et al.* The Effect of External Ventricular Drain Use in Intracerebral Hemorrhage. *World Neurosurg* **94**, 309–318 (2016).
6. Herrick, D. B. *et al.* Determinants of external ventricular drain placement and associated outcomes in patients with spontaneous intraventricular hemorrhage. *Neurocrit Care* **21**, 426–434 (2014).
7. Hanley, D. F. *et al.* Thrombolytic removal of intraventricular haemorrhage in treatment of severe stroke: results of the randomised, multicentre, multiregion, placebo-controlled CLEAR III trial. *Lancet* **389**, 603–611 (2017).
8. Akinduro, O. O. *et al.* Predictors of Ventriculoperitoneal shunting following Subarachnoid Hemorrhage treated with External Ventricular Drainage. *Neurocrit Care* **32**, 755–764 (2020).
9. Sadegh, C. *et al.* Choroid plexus-targeted NKCC1 overexpression to treat post-hemorrhagic hydrocephalus. *Neuron* **111**, 1591-1608.e4 (2023).
10. Karimy, J. K. *et al.* Inflammation-dependent cerebrospinal fluid hypersecretion by the choroid plexus epithelium in posthemorrhagic hydrocephalus. *Nat Med* **23**, 997–1003 (2017).
11. Garton, T. *et al.* Intraventricular Hemorrhage: the Role of Blood Components in Secondary Injury and Hydrocephalus. *Transl Stroke Res* **7**, 447–451 (2016).
12. Wang, Y. *et al.* Irisin ameliorates neuroinflammation and neuronal apoptosis through integrin αVβ5/AMPK signaling pathway after intracerebral hemorrhage in mice. *J Neuroinflammation* **19**, 82 (2022).

690 13. Shen, J. *et al*. Neurogenesis after primary intracerebral hemorrhage in adult human brain. *J Cereb Blood*
691 *Flow Metab* **28**, 1460–1468 (2008).
692 14. Xiong, X.-Y. & Yang, Q.-W. Rethinking the roles of inflammation in the intracerebral hemorrhage. *Transl*
693 *Stroke Res* **6**, 339–341 (2015).
694 15. Moraes, L. *et al*. Immune cells subpopulations in cerebrospinal fluid and peripheral blood of patients
695 with Aneurysmal Subarachnoid Hemorrhage. *Springerplus* **4**, 195 (2015).
696 16. Wigerblad, G. *et al*. Single-Cell Analysis Reveals the Range of Transcriptional States of Circulating
697 Human Neutrophils. *J Immunol* **209**, 772–782 (2022).
698 17. Gungabeesoon, J. *et al*. A neutrophil response linked to tumor control in immunotherapy. *Cell* **186**,
699 1448-1464.e20 (2023).
700 18. Sinha, S. *et al*. Dexamethasone modulates immature neutrophils and interferon programming in severe
701 COVID-19. *Nat Med* **28**, 201–211 (2022).
702 19. Kwok, A. J. *et al*. Neutrophils and emergency granulopoiesis drive immune suppression and an extreme
703 response endotype during sepsis. *Nat Immunol* **24**, 767–779 (2023).
704 20. Zhang, X., Tang, X., Liu, K., Hamblin, M. H. & Yin, K.-J. Long Noncoding RNA Malat1 Regulates
705 Cerebrovascular Pathologies in Ischemic Stroke. *J Neurosci* **37**, 1797–1806 (2017).
706 21. Pan, Y. *et al*. Novel Insights into the Emerging Role of Neat1 and Its Effects Downstream in the
707 Regulation of Inflammation. *J Inflamm Res* **15**, 557–571 (2022).
708 22. Agarwal, S. *et al*. The long non-coding RNA LUCAT1 is a negative feedback regulator of interferon
709 responses in humans. *Nat Commun* **11**, 6348 (2020).
710 23. Vierbuchen, T. *et al*. The lncRNA LUCAT1 is elevated in inflammatory disease and restrains
711 inflammation by regulating the splicing and stability of NR4A2. *Proceedings of the National Academy*
712 *of Sciences* **120**, e2213715120 (2023).
713 24. Xu, X. *et al*. GPCR-mediated PLCβγ/PKCβ/PKD signaling pathway regulates the cofilin phosphatase
714 slingshot 2 in neutrophil chemotaxis. *Mol Biol Cell* **26**, 874–886 (2015).

715 25. Kunisaki, Y. *et al.* DOCK2 is a Rac activator that regulates motility and polarity during neutrophil
716 chemotaxis. *J Cell Biol* **174**, 647–652 (2006).
717 26. Strieter, R. M. *et al.* Cytokine-induced neutrophil-derived interleukin-8. *Am J Pathol* **141**, 397–407
718 (1992).
719 27. Abdollahpour, H. *et al.* The phenotype of human STK4 deficiency. *Blood* **119**, 3450–3457 (2012).
720 28. Hu, T. *et al.* Single-cell analysis defines highly specific leukemia-induced neutrophils and links MMP8
721 expression to recruitment of tumor associated neutrophils during FGFR1 driven leukemogenesis. *Exp*
722 *Hematol Oncol* **13**, 49 (2024).
723 29. Hoogendijk, A. J. *et al.* Kinase activity is impaired in neutrophils of sepsis patients. *Haematologica* **104**,
724 e233–e235 (2019).
725 30. Goss, K. *et al.* Single-cell RNA-sequencing of circulating eosinophils from asthma patients reveals an
726 inflammatory signature. *iScience* **28**, 112609 (2025).
727 31. Guarda, G. *et al.* Type I interferon inhibits interleukin-1 production and inflammasome activation.
728 *Immunity* **34**, 213–223 (2011).
729 32. Mulder, K. *et al.* Cross-tissue single-cell landscape of human monocytes and macrophages in health
730 and disease. *Immunity* **54**, 1883-1900.e5 (2021).
731 33. Masuda, A. *et al.* Versican is upregulated in circulating monocytes in patients with systemic sclerosis
732 and amplifies a CCL2-mediated pathogenic loop. *Arthritis Res Ther* **15**, R74 (2013).
733 34. Wight, T. N., Kang, I. & Merrilees, M. J. Versican and the control of inflammation. *Matrix Biol* **35**, 152–
734 161 (2014).
735 35. Chang, M. Y. *et al.* Versican is produced by Trif- and type I interferon-dependent signaling in
736 macrophages and contributes to fine control of innate immunity in lungs. *Am J Physiol Lung Cell Mol*
737 *Physiol* **313**, L1069–L1086 (2017).
738 36. Wong, K. L. *et al.* Gene expression profiling reveals the defining features of the classical, intermediate,
739 and nonclassical human monocyte subsets. *Blood* **118**, e16–e31 (2011).

740 37. LeCouter, J., Zlot, C., Tejada, M., Peale, F. & Ferrara, N. Bv8 and endocrine gland-derived vascular
741 endothelial growth factor stimulate hematopoiesis and hematopoietic cell mobilization. *Proc Natl*
742 *Acad Sci U S A* **101**, 16813–16818 (2004).
743 38. Martucci, C. *et al*. Bv8, the amphibian homologue of the mammalian prokineticins, induces a
744 proinflammatory phenotype of mouse macrophages. *Br J Pharmacol* **147**, 225–234 (2006).
745 39. Shojaei, F. *et al*. Bv8 regulates myeloid-cell-dependent tumour angiogenesis. *Nature* **450**, 825–831
746 (2007).
747 40. Severini, C. *et al*. Bv8/prokineticin 2 is involved in Aβ-induced neurotoxicity. *Sci Rep* **5**, 15301 (2015).
748 41. Ng, K. L. *et al*. Dependence of olfactory bulb neurogenesis on prokineticin 2 signaling. *Science* **308**,
749 1923–1927 (2005).
750 42. Mundim, M. V. *et al*. A new function for Prokineticin 2: Recruitment of SVZ-derived neuroblasts to the
751 injured cortex in a mouse model of traumatic brain injury. *Mol Cell Neurosci* **94**, 1–10 (2019).
752 43. Zlotnik, A. & Yoshie, O. The chemokine superfamily revisited. *Immunity* **36**, 705–716 (2012).
753 44. Liu, C. *et al*. Chronic Stress Stimulates Protumor Macrophage Polarization to Propel Lung Cancer
754 Progression. *Cancer Res* **85**, 2429–2447 (2025).
755 45. Fan, Y. *et al*. The effect of anti-inflammatory properties of ferritin light chain on lipopolysaccharide-
756 induced inflammatory response in murine macrophages. *Biochim Biophys Acta* **1843**, 2775–2783
757 (2014).
758 46. Han, N.-R., Moon, P.-D., Kim, H.-M. & Jeong, H.-J. TSLP Exacerbates Septic Inflammation via Murine
759 Double Minute 2 (MDM2) Signaling Pathway. *J Clin Med* **8**, 1350 (2019).
760 47. Marques, L., Negre-Salvayre, A., Costa, L. & Canonne-Hergaux, F. Iron gene expression profile in
761 atherogenic Mox macrophages. *Biochim Biophys Acta* **1862**, 1137–1146 (2016).
762 48. Xu, Y. *et al*. Identification of conserved and tissue-restricted transcriptional profiles for lipid associated
763 macrophages. *Commun Biol* **8**, 953 (2025).

764 49. Beuker, C. *et al.* Stroke induces disease-specific myeloid cells in the brain parenchyma and pia. *Nat*
765 *Commun* **13**, 945 (2022).
766 50. Jiang, C. *et al.* Immune changes in peripheral blood and hematoma of patients with intracerebral
767 hemorrhage. *FASEB J* **34**, 2774–2791 (2020).
768 51. Hao, Y. *et al.* Integrated analysis of multimodal single-cell data. *Cell* **184**, 3573-3587.e29 (2021).
769 52. Glatzel, A. *et al.* Patterns of chemokine receptor expression on peripheral blood gamma delta T
770 lymphocytes: strong expression of CCR5 is a selective feature of V delta 2/V gamma 9 gamma delta T
771 cells. *J Immunol* **168**, 4920–4929 (2002).
772 53. Cui, A. *et al.* Dictionary of immune responses to cytokines at single-cell resolution. *Nature* **625**, 377–
773 384 (2024).
774 54. Jin, S. *et al.* Inference and analysis of cell-cell communication using CellChat. *Nat Commun* **12**, 1088
775 (2021).
776 55. Jin, S., Plikus, M. V. & Nie, Q. CellChat for systematic analysis of cell–cell communication from single-
777 cell transcriptomics. *Nat Protoc* **20**, 180–219 (2025).
778 56. Grieshaber-Bouyer, R. & Nigrovic, P. A. Neutrophil Heterogeneity as Therapeutic Opportunity in
779 Immune-Mediated Disease. *Front Immunol* **10**, 346 (2019).
780 57. Kamp, V. M. *et al.* Human suppressive neutrophils CD16bright/CD62Ldim exhibit decreased adhesion.
781 *J Leukoc Biol* **92**, 1011–1020 (2012).
782 58. Gusdon, A. M. *et al.* CSF and serum inflammatory response and association with outcomes in
783 spontaneous intracerebral hemorrhage with intraventricular extension: an analysis of the CLEAR-III
784 Trial. *J Neuroinflammation* **18**, 179 (2021).
785 59. Moxon-Emre, I. & Schlichter, L. C. Neutrophil depletion reduces blood-brain barrier breakdown, axon
786 injury, and inflammation after intracerebral hemorrhage. *J Neuropathol Exp Neurol* **70**, 218–235 (2011).
787 60. Provencio, J. J. *et al.* Neutrophil depletion after subarachnoid hemorrhage improves memory via NMDA
788 receptors. *Brain Behav Immun* **54**, 233–242 (2016).

789 61. Kenne, E., Erlandsson, A., Lindbom, L., Hillered, L. & Clausen, F. Neutrophil depletion reduces edema
790 formation and tissue loss following traumatic brain injury in mice. *J Neuroinflammation* **9**, 17 (2012).
791 62. Goods, B. A. *et al.* Leukocyte dynamics after intracerebral hemorrhage in a living patient reveal rapid
792 adaptations to tissue milieu. *JCI Insight* **6**, e145857, 145857 (2021).
793 63. Kawamura, Y. *et al.* Single-Cell Temporal Atlas of Myeloid Cells in the Live Haemorrhagic Brain.
794 2024.12.24.630187 Preprint at https://doi.org/10.1101/2024.12.24.630187 (2024).
795 64. Meng, N. *et al.* Single-cell transcriptomic landscape reveals the role of intermediate monocytes in
796 aneurysmal subarachnoid hemorrhage. *Front Cell Dev Biol* **12**, 1401573 (2024).
797 65. Sanchez, S. *et al.* Modulation of the Immunological Milieu in Acute Aneurysmal Subarachnoid
798 Hemorrhage: The Potential Role of Monocytes Through CXCL10 Secretion. *Transl Stroke Res* **16**, 88–95
799 (2025).
800 66. Xie, X. *et al.* Single-cell transcriptome profiling reveals neutrophil heterogeneity in homeostasis and
801 infection. *Nat Immunol* **21**, 1119–1133 (2020).
802 67. Haruna, N.-F. *et al.* scRNA-seq profiling of human granulocytes reveals expansion of developmentally
803 flexible neutrophil precursors with mixed neutrophil and eosinophil properties in asthma. *J Leukoc Biol*
804 **116**, 1184–1197 (2024).
805 68. Xiao, H. *et al.* High-throughput sequencing unravels the cell heterogeneity of cerebrospinal fluid in the
806 bacterial meningitis of children. *Front Immunol* **13**, 872832 (2022).
807 69. Askenase, M. H. *et al.* Longitudinal transcriptomics define the stages of myeloid activation in the living
808 human brain after intracerebral hemorrhage. *Sci Immunol* **6**, eabd6279 (2021).
809 70. Xu, H. *et al.* The choroid plexus synergizes with immune cells during neuroinflammation. *Cell* **187**,
810 4946-4963.e17 (2024).
811 71. Pak, C. B., Imanishi, J., Kishida, T. & Matsuo, A. Increased nitroblue tetrazolium dye reduction by human
812 neutrophils stimulated by interferon in vitro. *Microbiol Immunol* **24**, 717–723 (1980).

813 72. Benguigui, M. *et al.* Interferon-stimulated neutrophils as a predictor of immunotherapy response.
814 *Cancer Cell* **42**, 253-265.e12 (2024).
815 73. Chen, X. *et al.* Expression of costimulatory TNFR2 induces resistance of CD4+FoxP3- conventional T
816 cells to suppression by CD4+FoxP3+ regulatory T cells. *J Immunol* **185**, 174–182 (2010).
817 74. Seo, S.-U. *et al.* Type I Interferon Signaling Regulates Ly6Chi Monocytes and Neutrophils during Acute
818 Viral Pneumonia in Mice. *PLOS Pathogens* **7**, e1001304 (2011).
819 75. Nandi, B. & Behar, S. M. Regulation of neutrophils by interferon-γ limits lung inflammation during
820 tuberculosis infection. *J Exp Med* **208**, 2251–2262 (2011).
821 76. Kramer, A. H. *et al.* Intraventricular Fibrinolysis with Tissue Plasminogen Activator is Associated with
822 Transient Cerebrospinal Fluid Inflammation: A Randomized Controlled Trial. *J Cereb Blood Flow Metab*
823 **35**, 1241–1248 (2015).
824 77. Schmitz, T. *et al.* Interleukin-1β, Interleukin-18, and Interferon-γ Expression in the Cerebrospinal Fluid
825 of Premature Infants with Posthemorrhagic Hydrocephalus—Markers of White Matter Damage? *Pediatr*
826 *Res* **61**, 722–726 (2007).
827 78. Ekkert, A., Šliachtenko, A., Utkus, A. & Jatužis, D. Intracerebral Hemorrhage Genetics. *Genes (Basel)*
828 **13**, 1250 (2022).
829 79. Li, P. *et al.* rh-IFN-α Attenuates Neuroinflammation and Improves Neurological Function by Inhibiting
830 NF-κB through JAK1-STAT1/TRAF3 Pathway in an Experimental GMH Rat Model. *Brain Behav Immun* **79**,
831 174–185 (2019).
832 80. Vinukonda, G. *et al.* Intraventricular hemorrhage induces deposition of proteoglycans in premature
833 rabbits, but their in vivo degradation with chondroitinase does not restore myelination, ventricle size
834 and neurological recovery. *Exp Neurol* **247**, 630–644 (2013).
835 81. Bao, Z. *et al.* Prokineticin-2 prevents neuronal cell deaths in a model of traumatic brain injury. *Nat*
836 *Commun* **12**, 4220 (2021).

837 82. Thomas, A. J., Ogilvy, C. S., Griessenauer, C. J. & Hanafy, K. A. Macrophage CD163 expression in
838 cerebrospinal fluid: association with subarachnoid hemorrhage outcome. *J Neurosurg* **131**, 47–53
839 (2019).
840 83. de Graaf, M. T. *et al.* Central memory CD4+ T cells dominate the normal cerebrospinal fluid. *Cytometry*
841 *B Clin Cytom* **80**, 43–50 (2011).
842 84. Kivisäkk, P. *et al.* Human cerebrospinal fluid central memory CD4+ T cells: evidence for trafficking
843 through choroid plexus and meninges via P-selectin. *Proc Natl Acad Sci U S A* **100**, 8389–8394 (2003).
844 85. Peng, M. *et al.* Cell type hierarchy reconstruction via reconciliation of multi-resolution cluster tree.
845 *Nucleic Acids Res* **49**, e91 (2021).
846 86. Uhlen, M. *et al.* A genome-wide transcriptomic analysis of protein-coding genes in human blood cells.
847 *Science* **366**, eaax9198 (2019).
848 87. Karlsson, M. *et al.* A single-cell type transcriptomics map of human tissues. *Sci Adv* **7**, eabh2169
849 (2021).
850 88. The Human Protein Atlas. https://www.proteinatlas.org/.
851 89. Wildermuth, E. *et al.* A single-cell genomic atlas for the effects of chronic ethanol exposure in the
852 mouse dorsal striatum. *Mol Psychiatry* https://doi.org/10.1038/s41380-025-03014-z (2025)
853 doi:10.1038/s41380-025-03014-z.
854 90. Linderman, G. C. *et al.* Zero-preserving imputation of single-cell RNA-seq data. *Nat Commun* **13**, 192
855 (2022).
856 91. Orvis, J. *et al.* gEAR: Gene Expression Analysis Resource portal for community-driven, multi-omic data
857 exploration. *Nat Methods* **18**, 843–844 (2021).
858

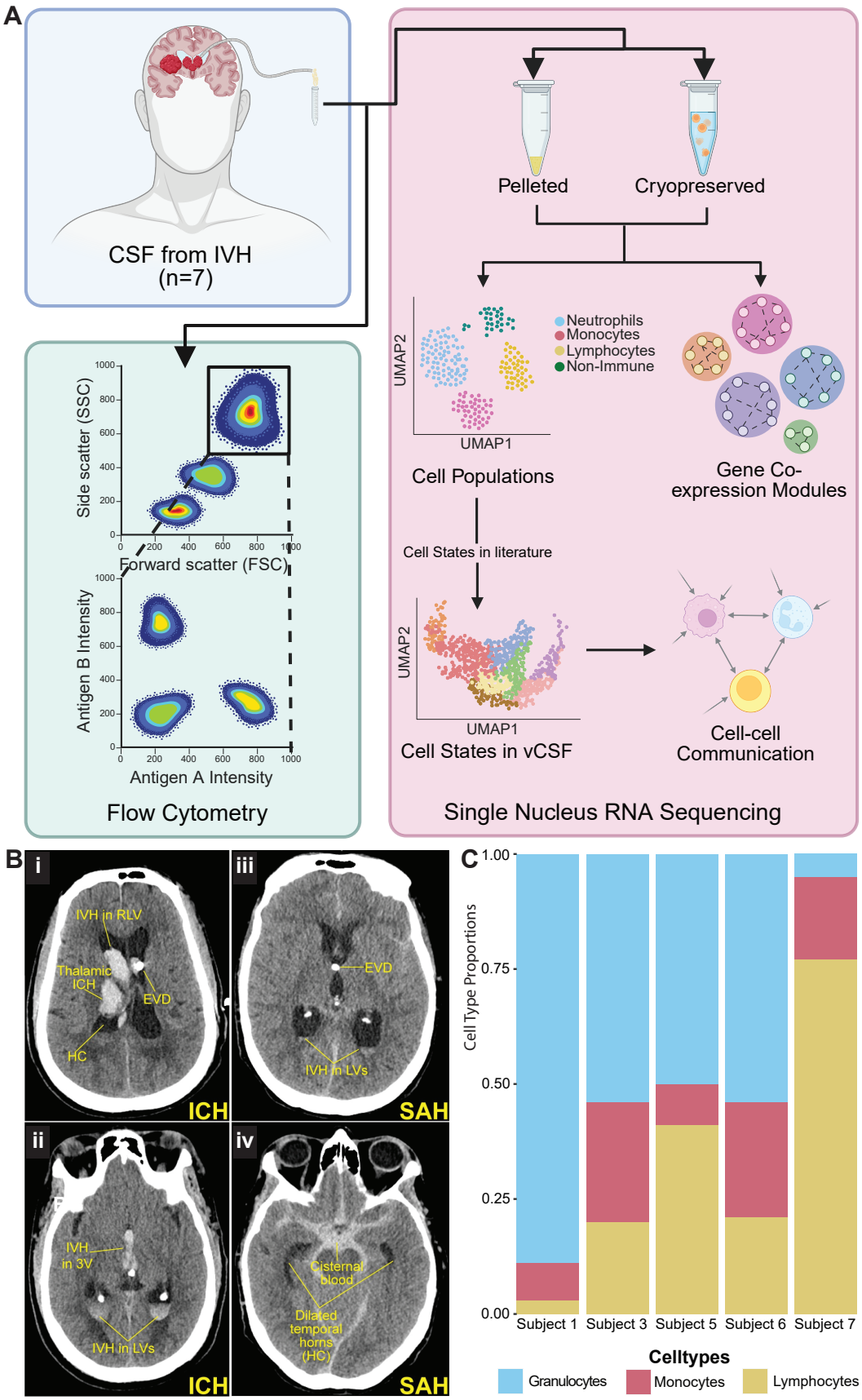
A
CSF from IVH
(n=7)
Pelleted
Cryopreserved
Side scatter (SSC)
Forward scatter (FSC)
Antigen B Intensity
Antigen A Intensity
Flow Cytometry
UMAP2
UMAP1
Neutrophils
Monocytes
Lymphocytes
Non-Immune
Cell Populations
Gene Co-expression Modules
Cell States in literature
Cell States in vCSF
Cell-cell Communication
Single Nucleus RNA Sequencing
B
i
IVH in RLV
Thalamic ICH
EVD
HC
ICH
iii
EVD
IVH in LVs
SAH
ii
IVH in 3V
IVH in LVs
ICH
iv
Cisternal blood
Dilated temporal horns (HC)
SAH
C
Cell Type Proportions
1.00
0.75
0.50
0.25
0.00
Subject 1
Subject 3
Subject 5
Subject 6
Subject 7
Celltypes
Granulocytes
Monocytes
Lymphocytes

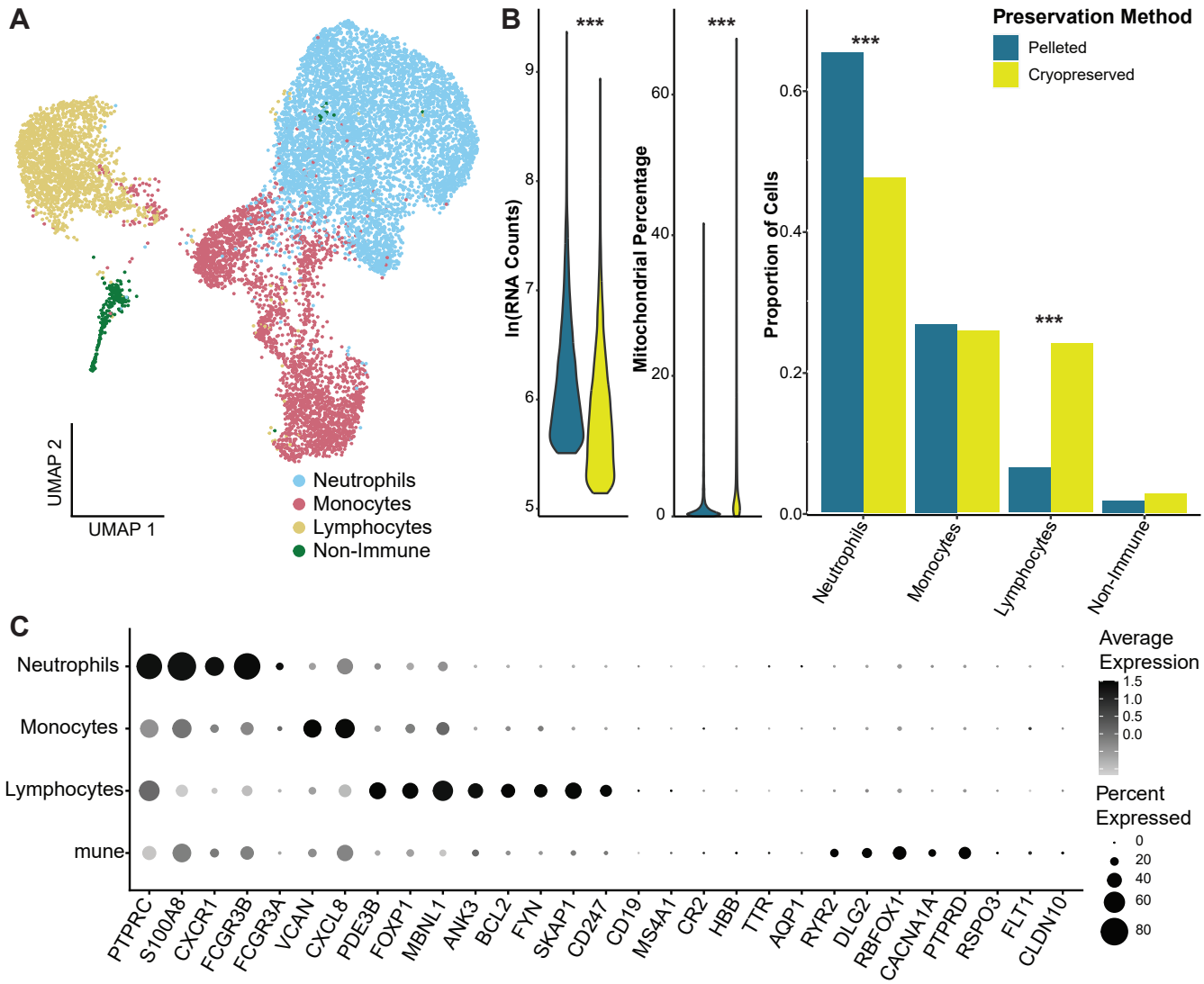
A
UMAP 2
UMAP 1
Neutrophils
Monocytes
Lymphocytes
Non-Immune
B
***
ln(RNA Counts)
Mitochondrial Percentage
Proportion of Cells
Preservation Method
Pelleted
Cryopreserved
Neutrophils
Monocytes
Lymphocytes
Non-Immune
C
Neutrophils
Monocytes
Lymphocytes
mune
PTPRC
S100A8
CXCR1
FCGR3B
FCGR3A
VCAN
CXCL8
PDE3B
FOXP1
MBNL1
ANK3
BCL2
FYN
SKAP1
CD247
CD19
MS4A1
CR2
HBB
TTR
AQP1
RYR2
DLG2
RBFOX1
CACNA1A
PTPRD
RSPO3
FLT1
CLDN10
Average Expression
Percent Expressed

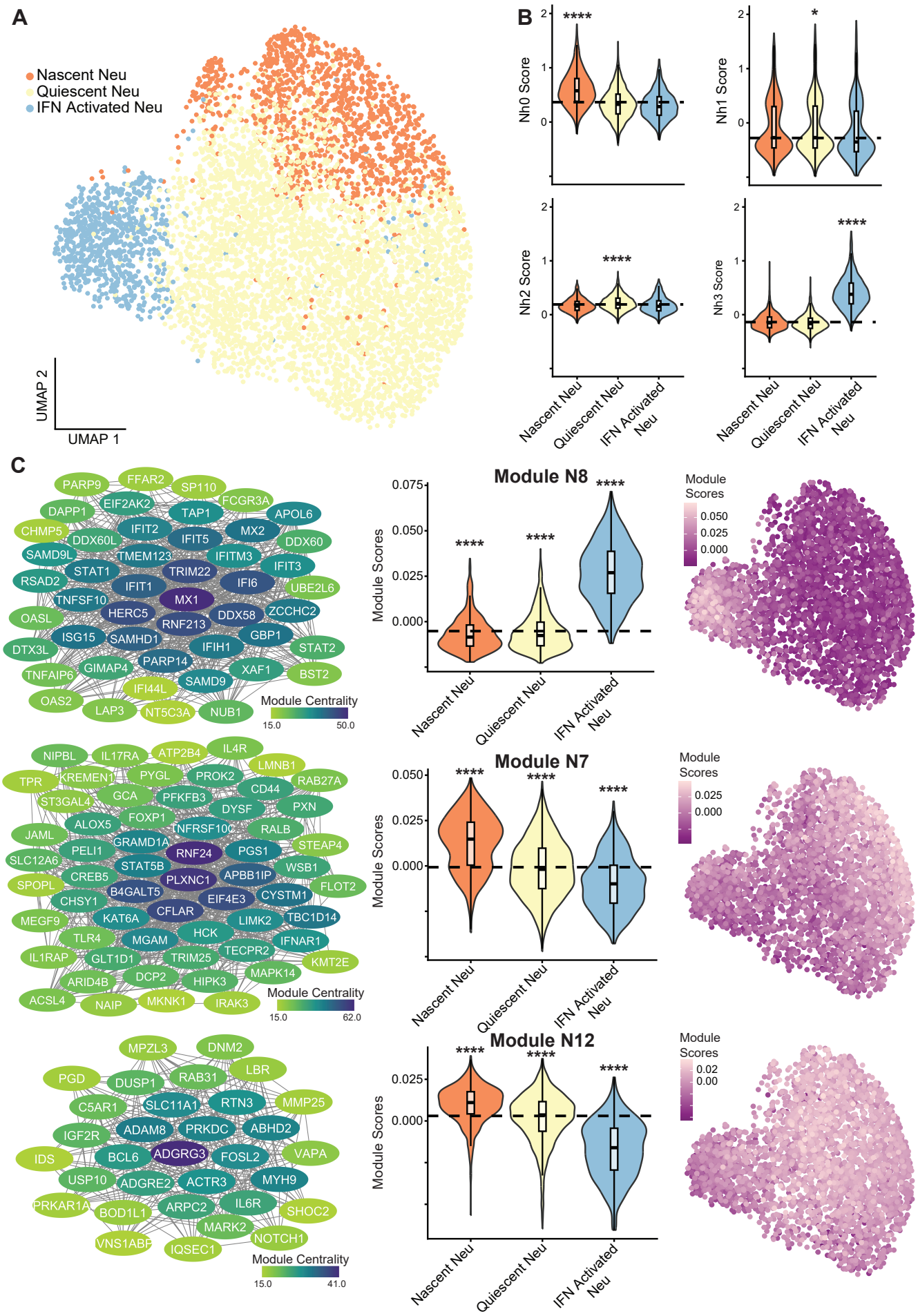
A
Nascent Neu
Quiescent Neu
IFN Activated Neu
UMAP 2
UMAP 1
B
Nh0 Score
Nh1 Score
Nh2 Score
Nh3 Score
Nascent Neu
Quiescent Neu
IFN Activated Neu
C
Module N8
Module N7
Module N12
Module Scores
Module Centrality
15.0
50.0
62.0
41.0

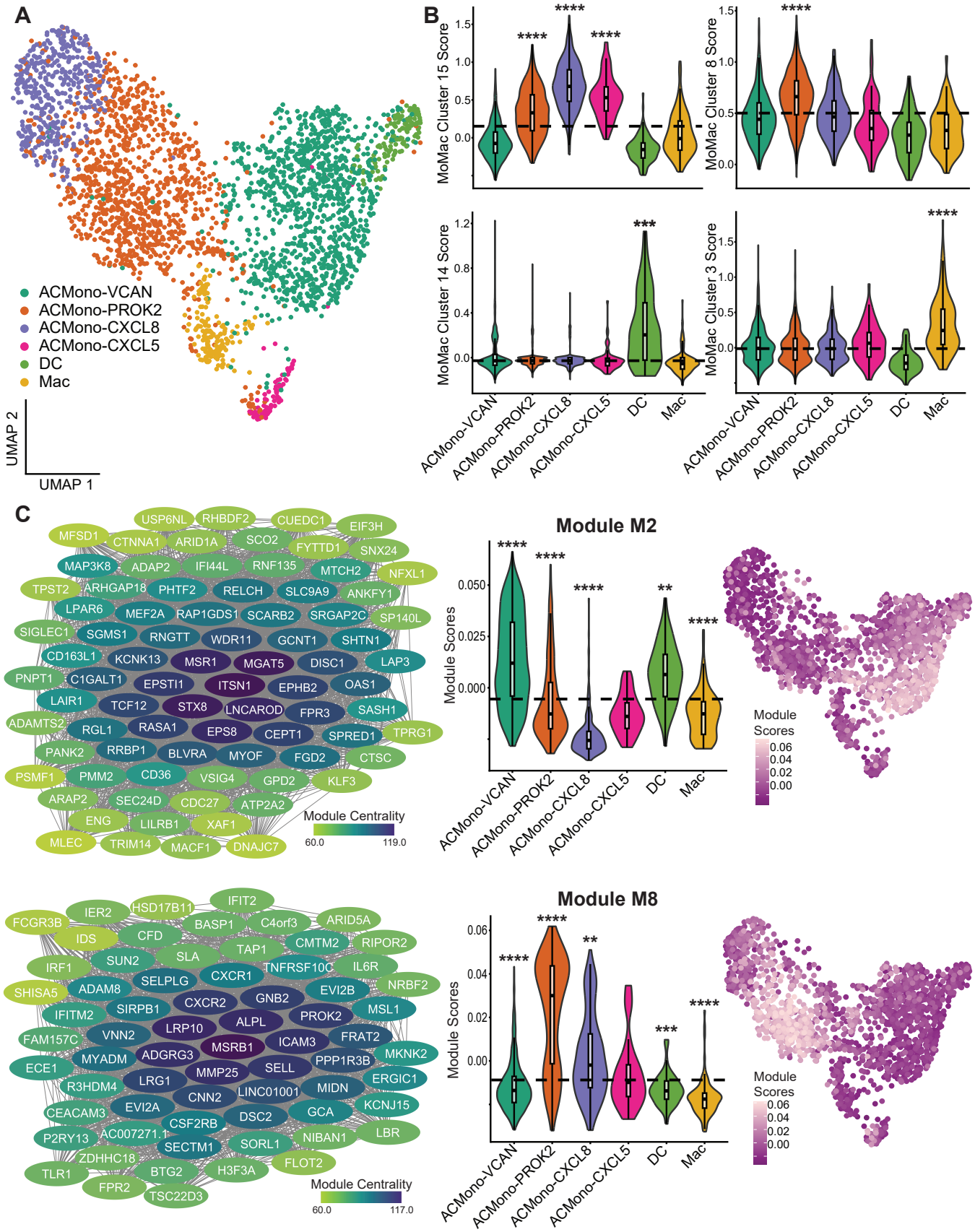
A
ACMono-VCAN
ACMono-PROK2
ACMono-CXCL8
ACMono-CXCL5
DC
Mac
UMAP 2
UMAP 1
B
MoMac Cluster 15 Score
MoMac Cluster 8 Score
MoMac Cluster 14 Score
MoMac Cluster 3 Score
ACMono-VCAN
ACMono-PROK2
ACMono-CXCL8
ACMono-CXCL5
DC
Mac
C
Module M2
Module Scores
Module Centrality
60.0
119.0
Module Scores
0.06
0.04
0.02
0.00
Module M8
Module Centrality
60.0
117.0

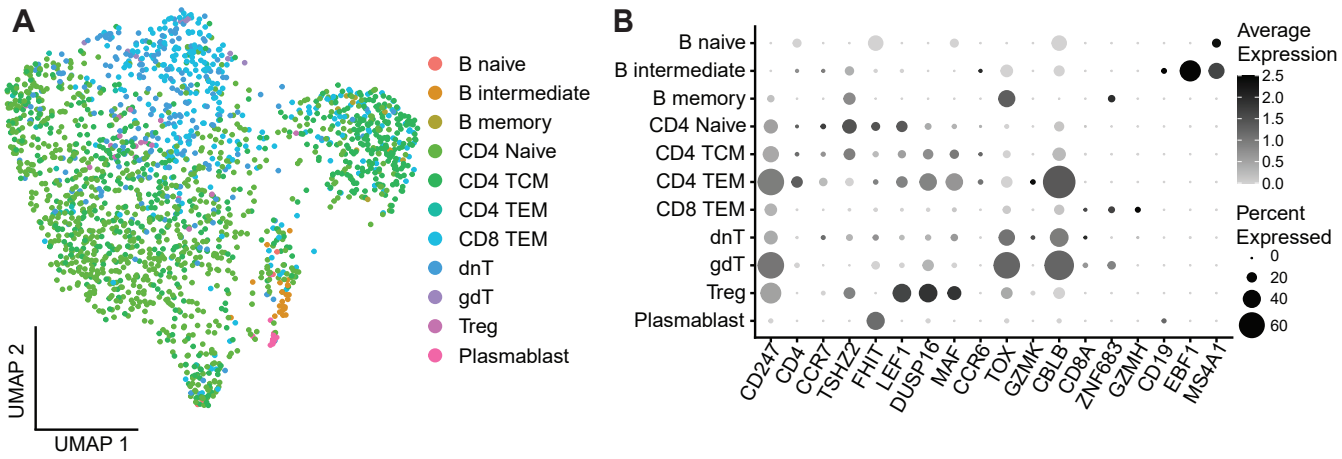
A
B naive
B intermediate
B memory
CD4 Naive
CD4 TCM
CD4 TEM
CD8 TEM
dnT
gdT
Treg
Plasmablast
UMAP 2
UMAP 1
B
B naive
B intermediate
B memory
CD4 Naive
CD4 TCM
CD4 TEM
CD8 TEM
dnT
gdT
Treg
Plasmablast
CD24T
CD4
CCR7
TSHZ2
FHIT
LEF1
DUSP16
MAF
CCR6
TOX
GZMK
CBLB
CD8A
ZNF683
GZMH
CD19
EBF1
MS4A1
Average Expression
2.5
2.0
1.5
1.0
0.5
0.0
Percent Expressed
0
20
40
60

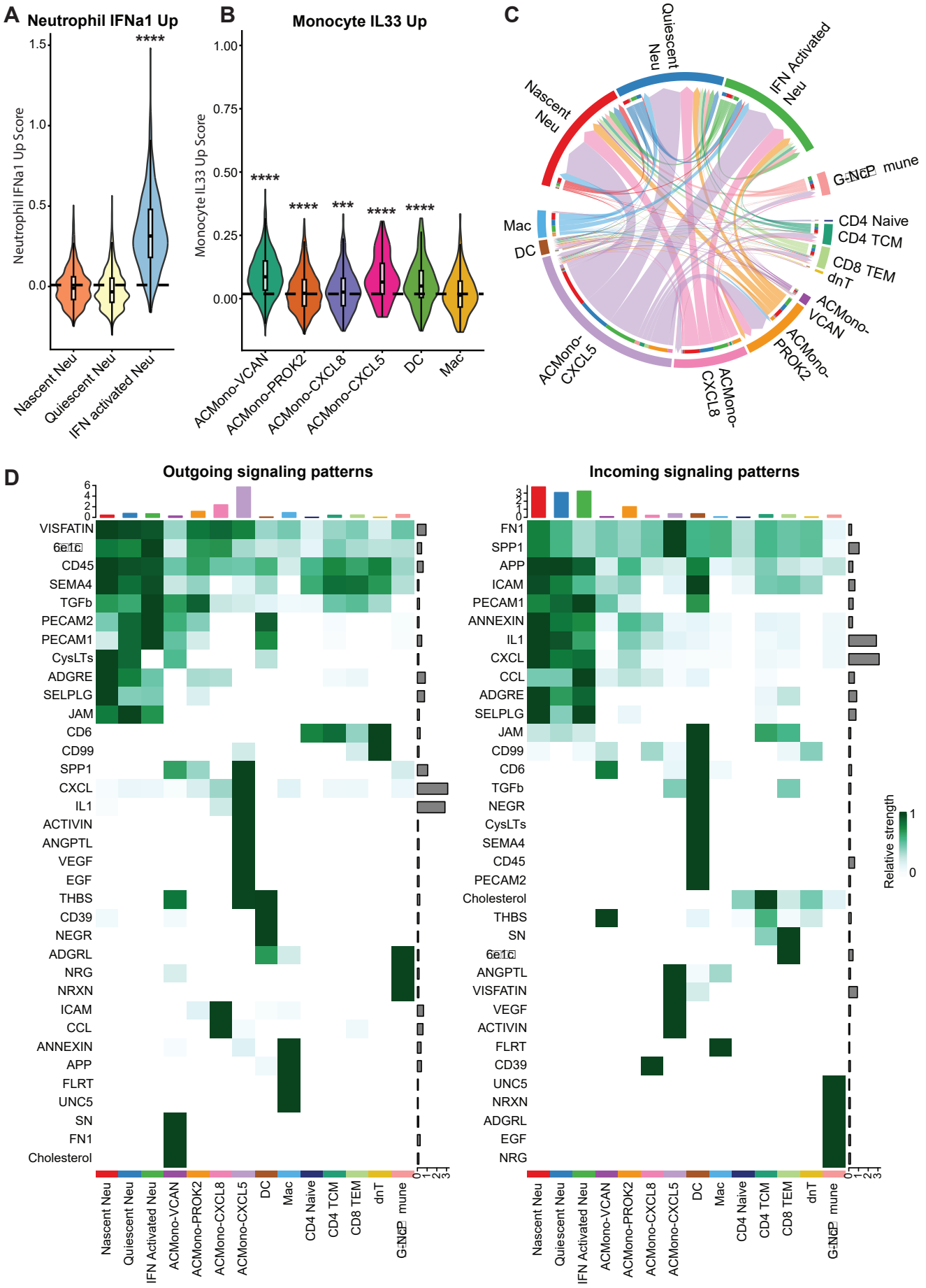
A
Neutrophil IFNa1 Up
Neutrophil IFNa1 Up Score
Nascent Neu
Quiescent Neu
IFN activated Neu
B
Monocyte IL33 Up
Monocyte IL33 Up Score
ACMono-VCAN
ACMono-PROK2
ACMono-CXCL8
ACMono-CXCL5
DC
Mac
C
Quiescent Neu
IFN Activated Neu
Nascent Neu
Mac
DC
CD4 Naive
CD4 TCM
CD8 TEM
dnT
ACMono-VCAN
ACMono-PROK2
ACMono-CXCL8
ACMono-CXCL5
D
Outgoing signaling patterns
Incoming signaling patterns
Relative strength

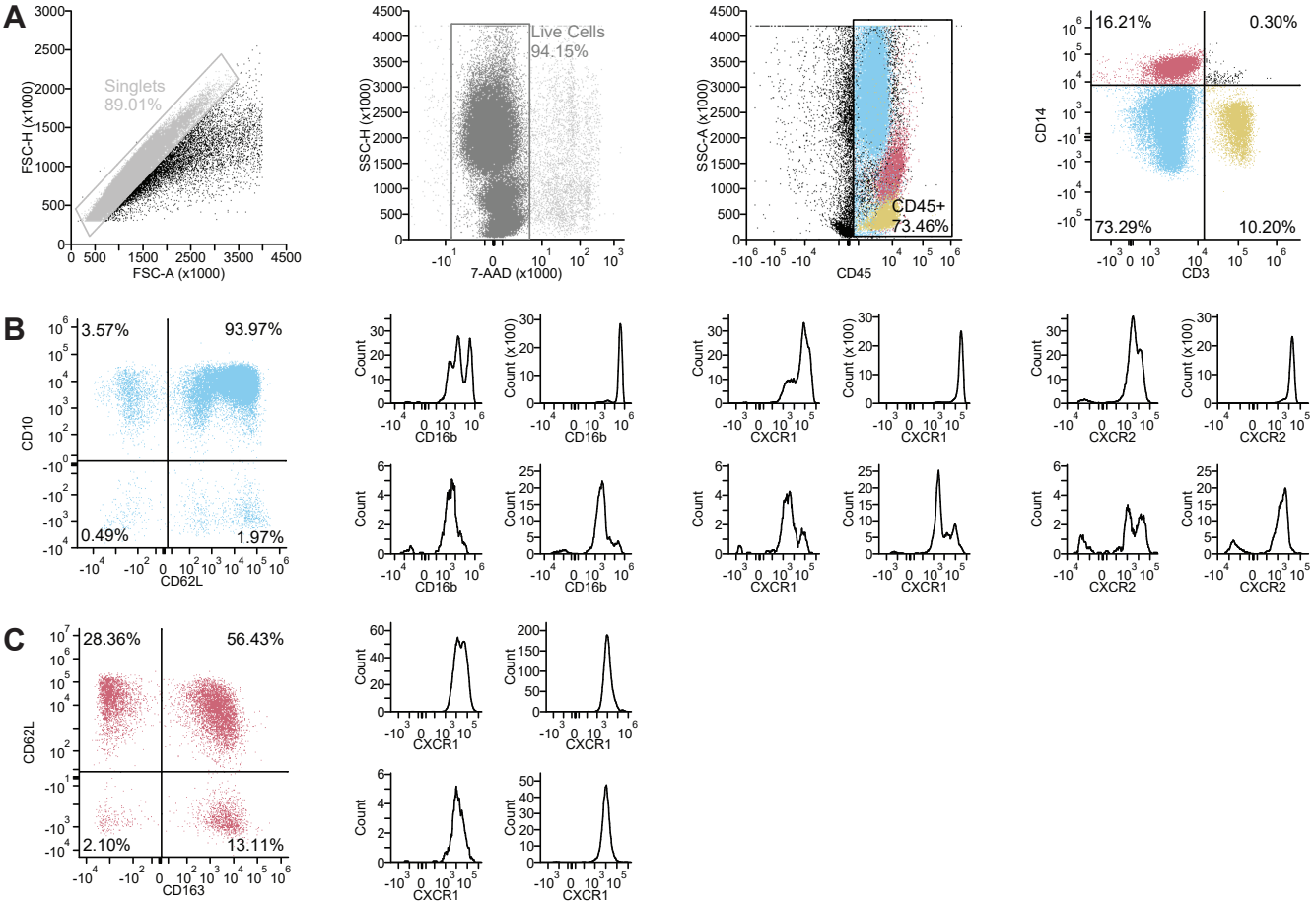
A
Singlets
89.01%
FSC-H (x1000)
FSC-A (x1000)
Live Cells
94.15%
SSC-H (x1000)
7-AAD (x1000)
CD45+
73.46%
SSC-A (x1000)
CD45
16.21%
0.30%
73.29%
10.20%
CD14
CD3
B
3.57%
93.97%
0.49%
1.97%
CD10
CD62L
Count
Count (x100)
CD16b
CXCR1
CXCR2
C
28.36%
56.43%
2.10%
13.11%
CD62L
CD163
Count
CXCR1

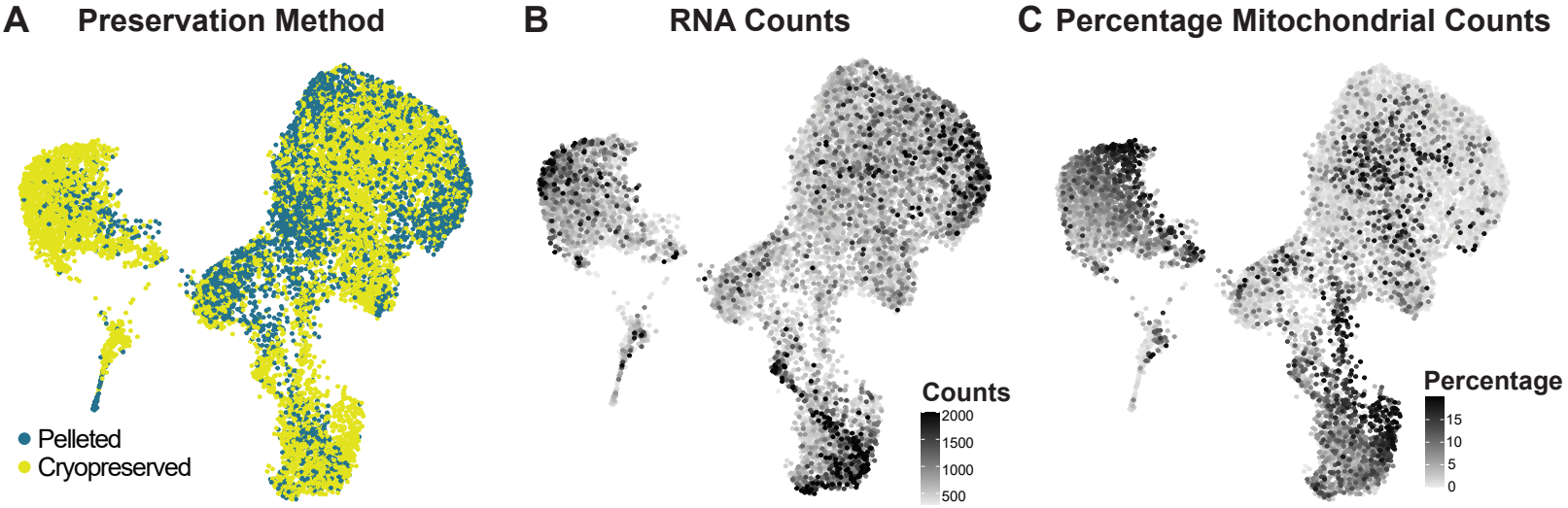
A
Preservation Method
Pelleted
Cryopreserved
B
RNA Counts
Counts
2000
1500
1000
500
C
Percentage Mitochondrial Counts
Percentage
15
10
5
0

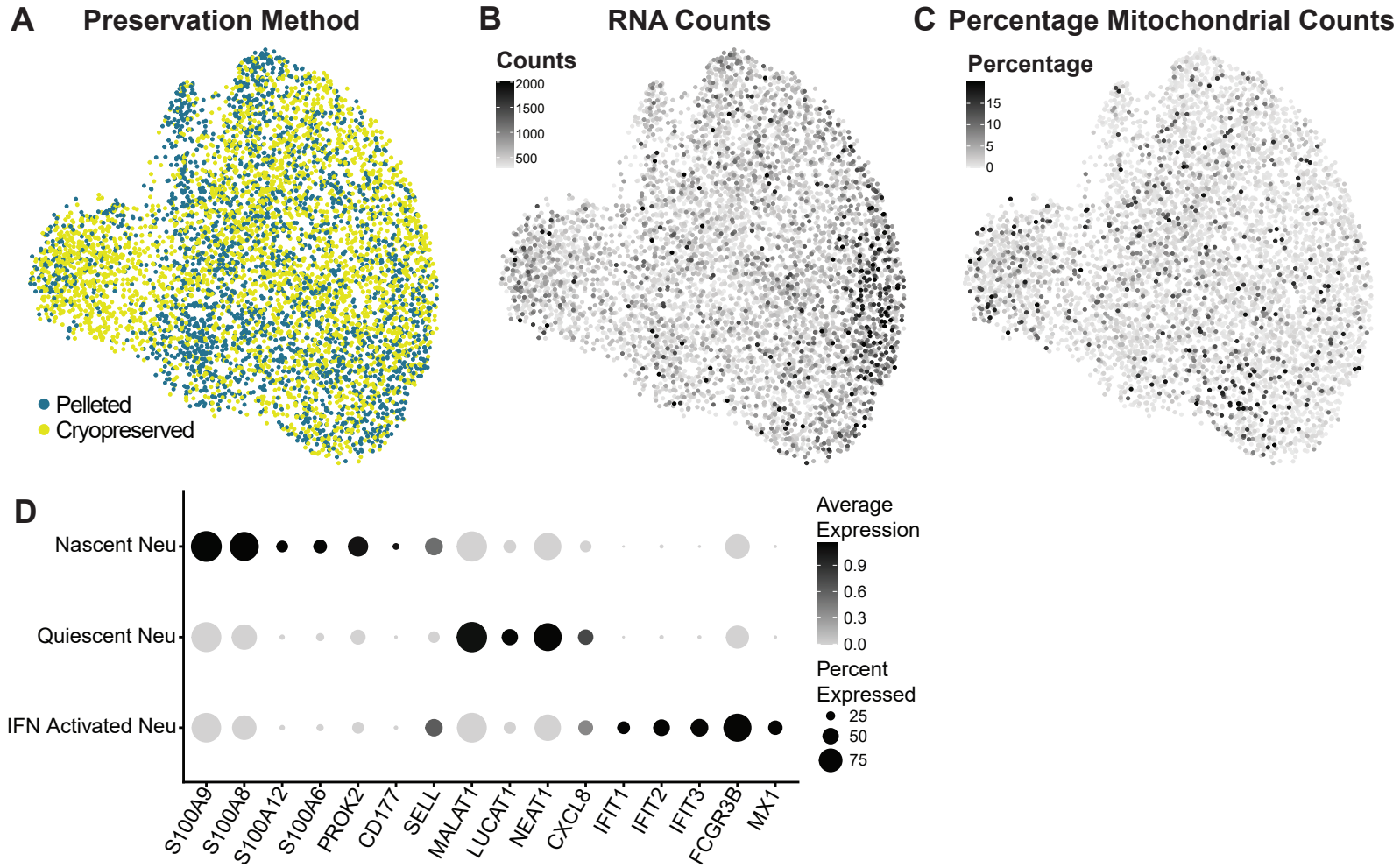
A
Preservation Method
Pelleted
Cryopreserved
B
RNA Counts
Counts
2000
1500
1000
500
C
Percentage Mitochondrial Counts
Percentage
15
10
5
0
D
Nascent Neu
Quiescent Neu
IFN Activated Neu
S100A9
S100A8
S100A12
S100A6
PROK2
CD177
SELL
MALAT1
LUCAT1
NEAT1
CXCL8
IFIT1
IFIT2
IFIT3
FCGR3B
MX1
Average Expression
0.9
0.6
0.3
0.0
Percent Expressed
25
50
75

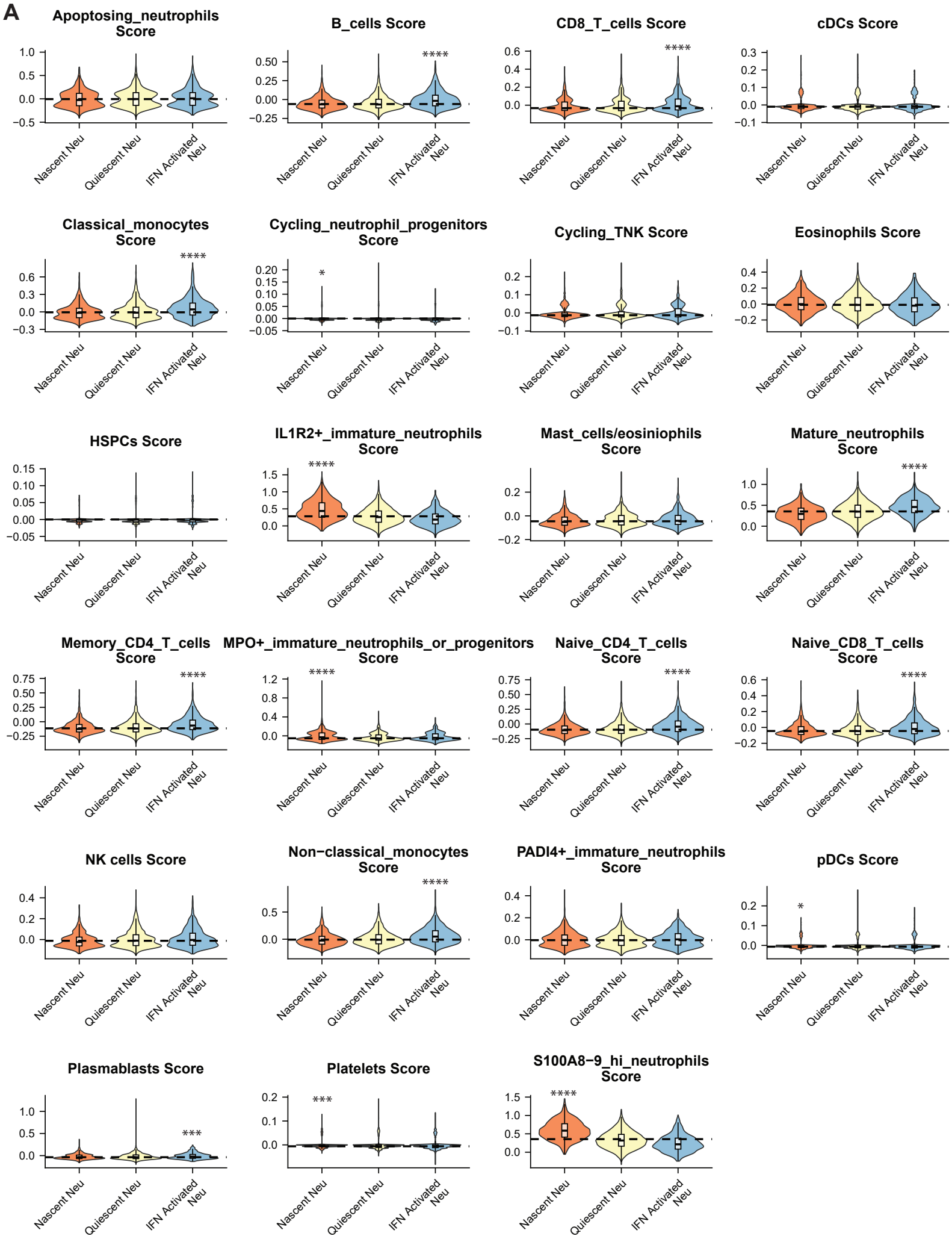
A
Apoptosing_neutrophils Score
B_cells Score
CD8_T_cells Score
cDCs Score
Classical_monocytes Score
Cycling_neutrophil_progenitors Score
Cycling_TNK Score
Eosinophils Score
HSPCs Score
IL1R2+_immature_neutrophils Score
Mast_cells/eosiniophils Score
Mature_neutrophils Score
Memory_CD4_T_cells Score
MPO+_immature_neutrophils_or_progenitors Score
Naive_CD4_T_cells Score
Naive_CD8_T_cells Score
NK cells Score
Non−classical_monocytes Score
PADI4+_immature_neutrophils Score
pDCs Score
Plasmablasts Score
Platelets Score
S100A8−9_hi_neutrophils Score
Nascent Neu
Quiescent Neu
IFN Activated Neu

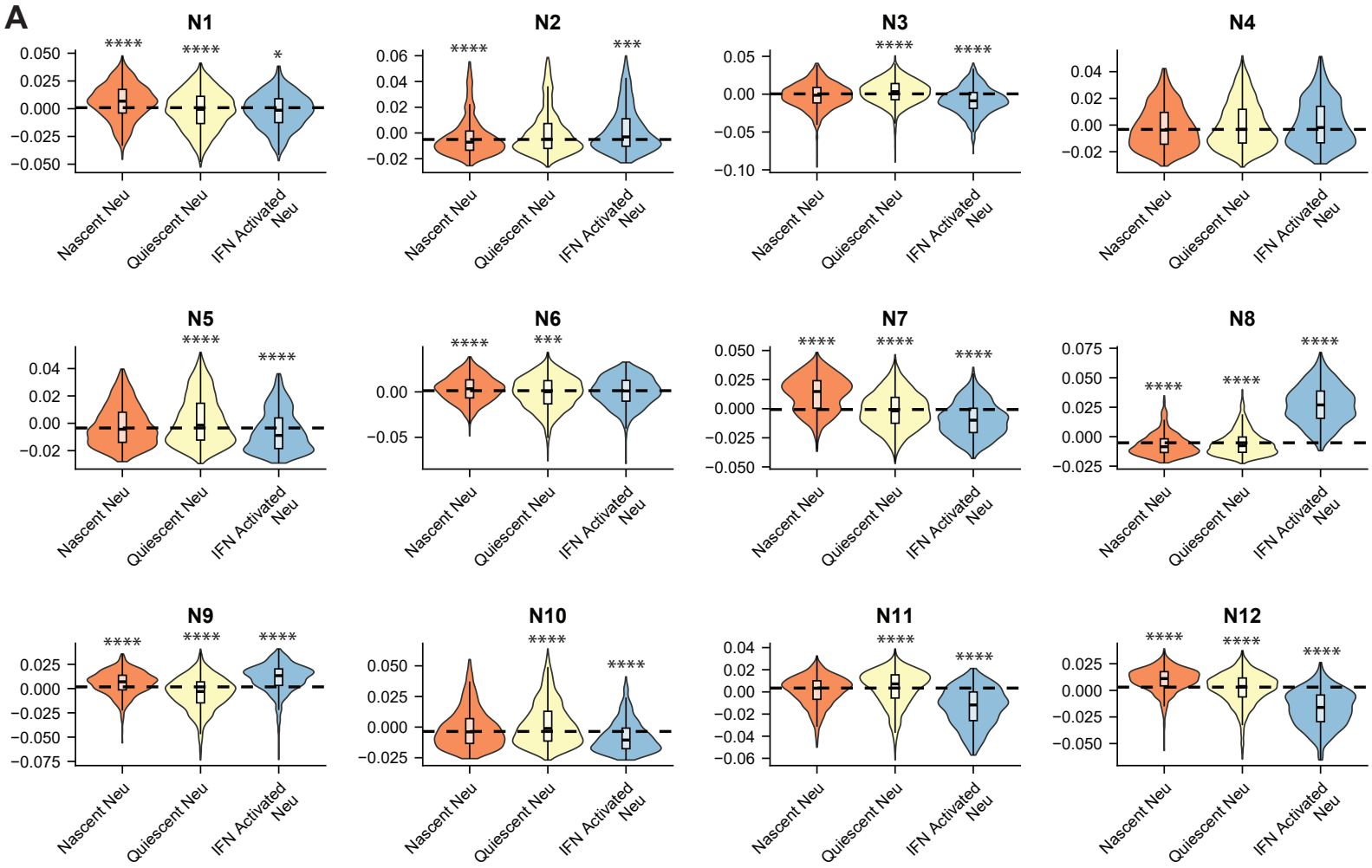
A
N1
N2
N3
N4
N5
N6
N7
N8
N9
N10
N11
N12
Nascent Neu
Quiescent Neu
IFN Activated Neu

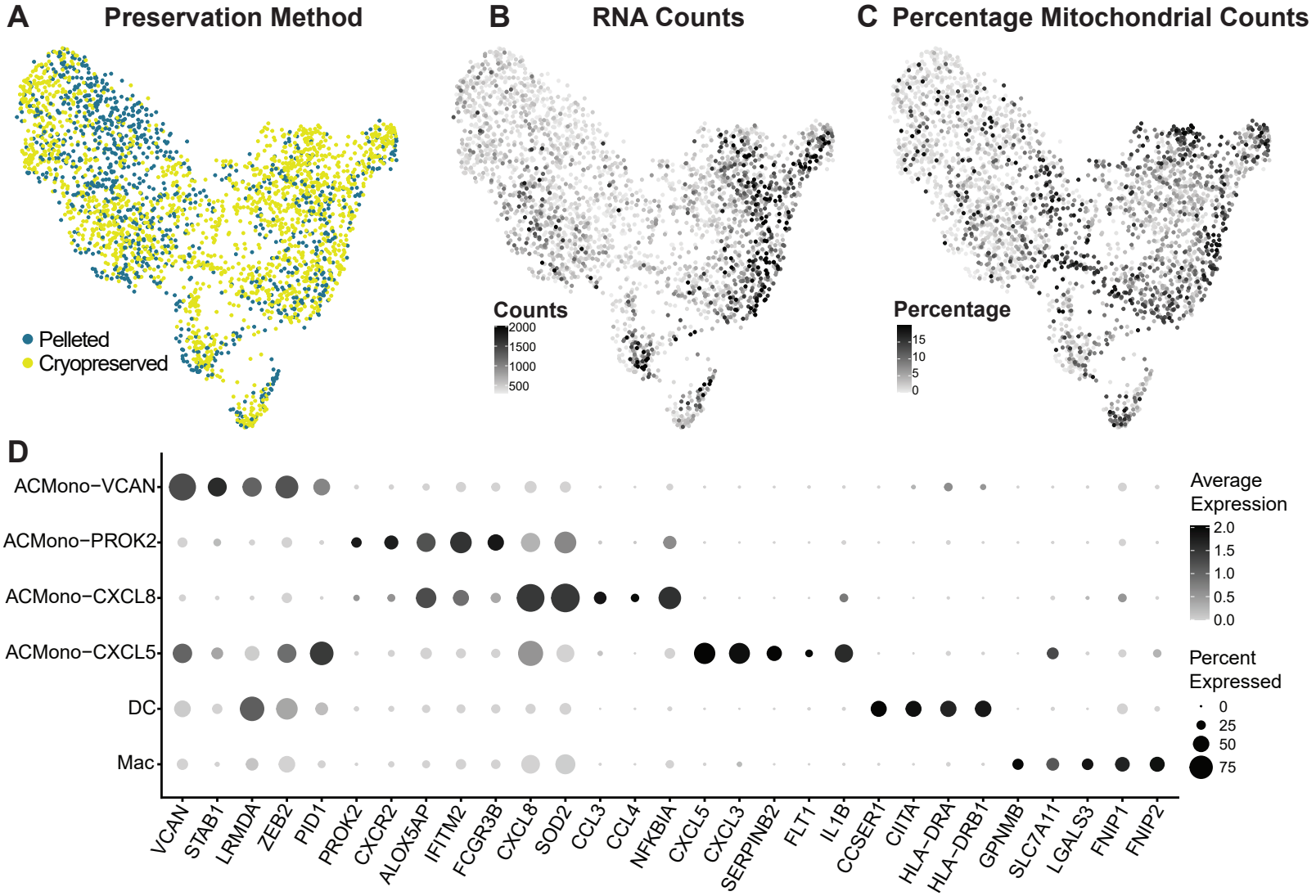
A
Preservation Method
Pelleted
Cryopreserved
B
RNA Counts
Counts
2000
1500
1000
500
C
Percentage Mitochondrial Counts
Percentage
15
10
5
0
D
ACMono−VCAN
ACMono−PROK2
ACMono−CXCL8
ACMono−CXCL5
DC
Mac
VCAN
STAB1
LRMDA
ZEB2
PID1
PROK2
CXCR2
ALOX5AP
IFITM2
FCGR3B
CXCL8
SOD2
CCL3
CCL4
NFKBIA
CXCL5
CXCL3
SERPINB2
FLT1
IL1B
CCSER1
CIITA
HLA−DRA
HLA−DRB1
GPNMB
SLC7A11
LGALS3
FNIP1
FNIP2
Average Expression
2.0
1.5
1.0
0.5
0.0
Percent Expressed
0
25
50
75

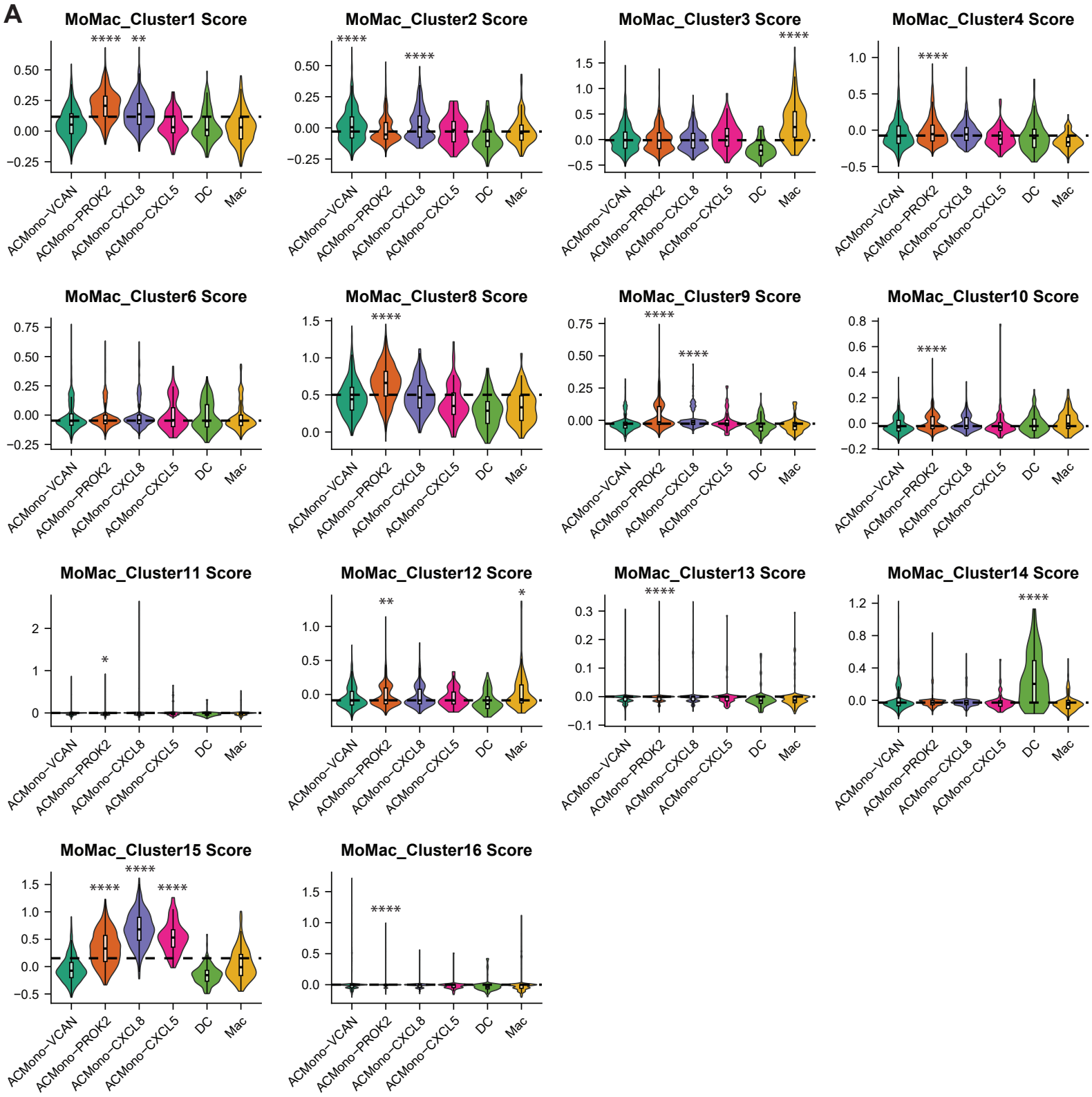
A
MoMac_Cluster1 Score
MoMac_Cluster2 Score
MoMac_Cluster3 Score
MoMac_Cluster4 Score
MoMac_Cluster6 Score
MoMac_Cluster8 Score
MoMac_Cluster9 Score
MoMac_Cluster10 Score
MoMac_Cluster11 Score
MoMac_Cluster12 Score
MoMac_Cluster13 Score
MoMac_Cluster14 Score
MoMac_Cluster15 Score
MoMac_Cluster16 Score
ACMono−VCAN
ACMono−PROK2
ACMono−CXCL8
ACMono−CXCL5
DC
Mac

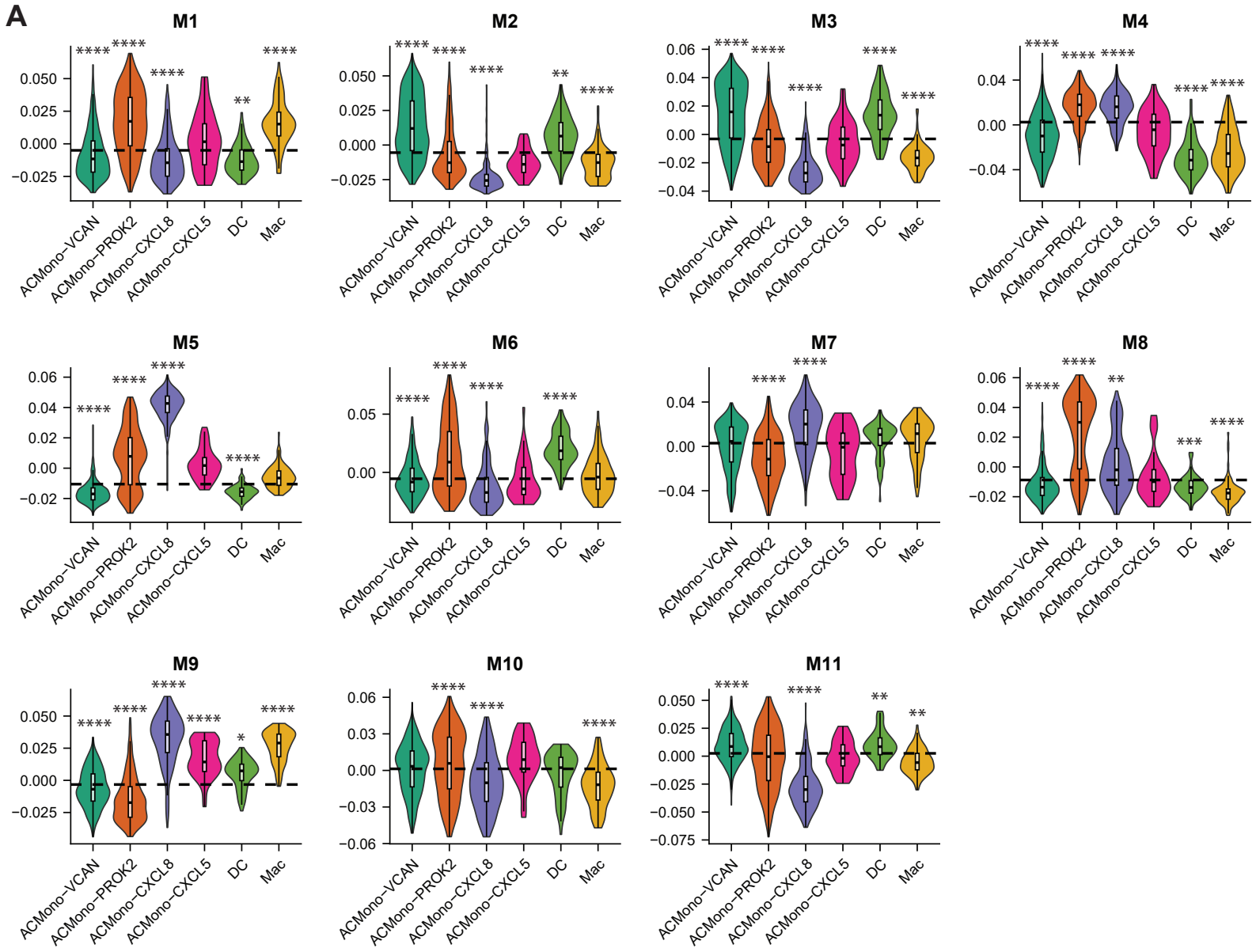
A
M1
M2
M3
M4
M5
M6
M7
M8
M9
M10
M11
ACMono-VCAN
ACMono-PROK2
ACMono-CXCL8
ACMono-CXCL5
DC
Mac

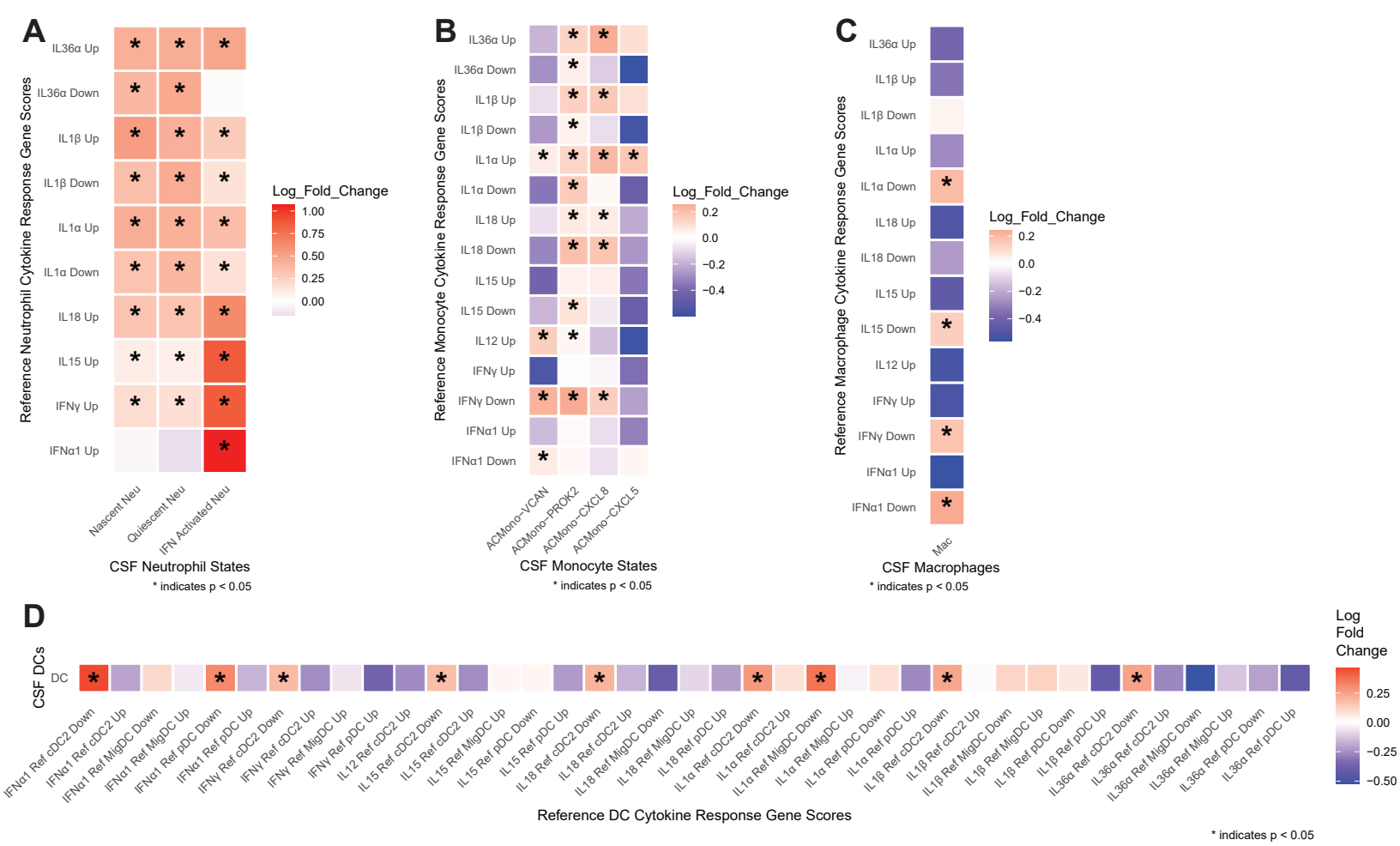
A
Reference Neutrophil Cytokine Response Gene Scores
IL36α Up
IL36α Down
IL1β Up
IL1β Down
IL1α Up
IL1α Down
IL18 Up
IL15 Up
IFNγ Up
IFNα1 Up
Nascent Neu
Quiescent Neu
IFN Activated Neu
CSF Neutrophil States
* indicates p < 0.05
Log_Fold_Change
1.00
0.75
0.50
0.25
0.00
B
Reference Monocyte Cytokine Response Gene Scores
IL36α Up
IL36α Down
IL1β Up
IL1β Down
IL1α Up
IL1α Down
IL18 Up
IL18 Down
IL15 Up
IL15 Down
IL12 Up
IFNγ Up
IFNγ Down
IFNα1 Up
IFNα1 Down
ACMono−VCAN
ACMono−PROK2
ACMono−CXCL8
ACMono−CXCL5
CSF Monocyte States
* indicates p < 0.05
Log_Fold_Change
0.2
0.0
−0.2
−0.4
C
Reference Macrophage Cytokine Response Gene Scores
IL36α Up
IL1β Up
IL1β Down
IL1α Up
IL1α Down
IL18 Up
IL18 Down
IL15 Up
IL15 Down
IL12 Up
IFNγ Up
IFNγ Down
IFNα1 Up
IFNα1 Down
Mac
CSF Macrophages
* indicates p < 0.05
Log_Fold_Change
0.2
0.0
−0.2
−0.4

D
CSF DCs
DC
IFNα1 Ref cDC2 Down
IFNα1 Ref cDC2 Up
IFNα1 Ref MigDC Down
IFNα1 Ref MigDC Up
IFNα1 Ref pDC Down
IFNα1 Ref pDC Up
IFNγ Ref cDC2 Down
IFNγ Ref cDC2 Up
IFNγ Ref MigDC Up
IFNγ Ref pDC Up
IL12 Ref cDC2 Up
IL15 Ref cDC2 Down
IL15 Ref cDC2 Up
IL15 Ref MigDC Up
IL15 Ref pDC Down
IL15 Ref pDC Up
IL18 Ref cDC2 Down
IL18 Ref cDC2 Up
IL18 Ref MigDC Down
IL18 Ref MigDC Up
IL18 Ref pDC Up
IL1α Ref cDC2 Down
IL1α Ref cDC2 Up
IL1α Ref MigDC Down
IL1α Ref MigDC Up
IL1α Ref pDC Down
IL1α Ref pDC Up
IL1β Ref cDC2 Down
IL1β Ref cDC2 Up
IL1β Ref MigDC Down
IL1β Ref MigDC Up
IL1β Ref pDC Down
IL1β Ref pDC Up
IL36α Ref cDC2 Down
IL36α Ref cDC2 Up
IL36α Ref MigDC Down
IL36α Ref MigDC Up
IL36α Ref pDC Down
IL36α Ref pDC Up
Reference DC Cytokine Response Gene Scores
* indicates p < 0.05
Log Fold Change
0.25
0.00
−0.25
−0.50

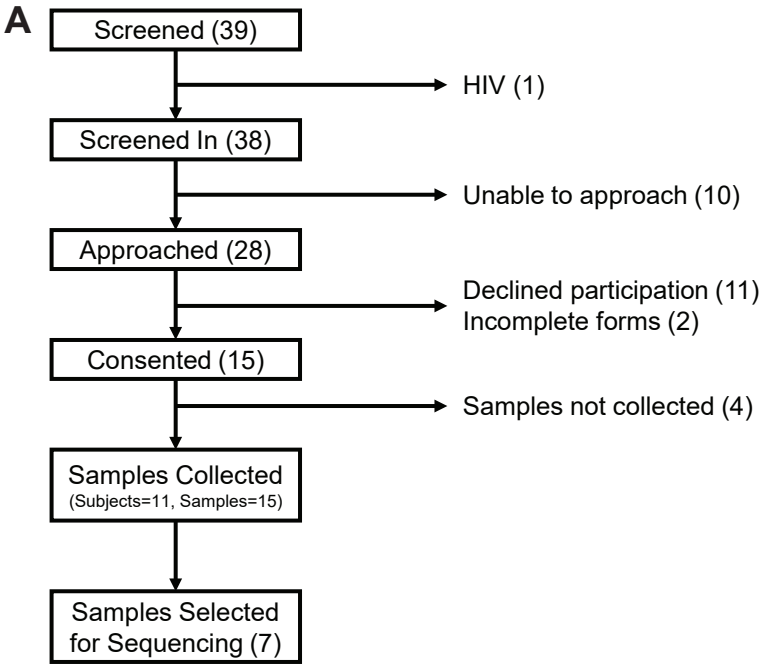
A
Screened (39)
HIV (1)
Screened In (38)
Unable to approach (10)
Approached (28)
Declined participation (11)
Incomplete forms (2)
Consented (15)
Samples not collected (4)
Samples Collected
(Subjects=11, Samples=15)
Samples Selected
for Sequencing (7)